Uncovering the electrical synapse proteome in retinal neurons via *in vivo* proximity labeling

Stephan Tetenborg[1,8], Eyad Shihabeddin[1,9], Elizebeth Olive Akansha Manoj Kumar[1,9], Crystal L. Sigulinsky[2,9], Karin Dedek[3,4], Ya-Ping Lin[1], Fabio A. Echeverry[5], Hannah Hoff[5], Alberto E. Pereda[5], Bryan W. Jones[2], Christophe P. Ribelayga[1], Klaus Ebnet[6], Ken Matsuura[7] & John O'Brien[1,8]

[1]College of Optometry, University of Houston, Houston, TX, United states.
[2]Moran Eye Center/Ophthalmology, University of Utah, Salt Lake City, Utah, United states.
[3]Animal Navigation/ Neurosensorics, Institute for Biology and Environmental Sciences, University of Oldenburg, Oldenburg, Germany.
[4]Research Center Neurosensory Science, University of Oldenburg, Oldenburg, Germany.
[5]Dominick P. Purpura Department of Neuroscience, Albert Einstein College of Medicine, Bronx, New York, United States.
[6]Institute-Associated Research Group: Cell Adhesion and Cell Polarity, Institute of Medical Biochemistry, ZMBE, University of Münster, Münster, Germany.
[7]Cell Signal Unit, Okinawa Institute of Science and Technology, Onna-son 904-0495, Japan.
[8]To whom correspondence should be addressed
[9]Contributed equally

Correspondence: stetenbo@Central.UH.EDU (S.T.) and jobrien3@Central.UH.EDU (J.OB.)

Research article, neuroscience

Keywords: TurboID, AII amacrine cell, Electrical Synapse, Connexin 36

The authors declare no competing interests.

Abstract

Electrical synapses containing Connexin 36 (Cx36) represent the main means for direct electrical communication among neurons in the mammalian nervous system. However, little is known about the protein complexes that constitute these synapses. In the present study, we applied different BioID strategies to screen the interactomes of Connexin 36 and its zebrafish orthologue Cx35b in retinal neurons. For *in vivo* proximity labeling in mice, we took advantage of the Cx36-EGFP strain and expressed a GFP-nanobody-TurboID fusion construct selectively in AII amacrine cells. For *in vivo* BioID in zebrafish, we generated a transgenic line expressing a Cx35b-TurboID fusion under control of the Cx35b promoter. Both strategies allowed us to capture a plethora of molecules that were associated with electrical synapses and showed a high degree of evolutionary conservation in the proteomes of both species. Besides known interactors of Cx36 such as ZO-1 and ZO-2 we have identified more than 50 new proteins, such as scaffold proteins, adhesion molecules and regulators of the cytoskeleton. Moreover, we determined the subcellular localization of these proteins in mouse retina and tested potential binding interactions with Cx36. Amongst these new interactors, we identified signal induced proliferation associated 1 like 3 (Sipa1l3), a protein that has been implicated in cell junction formation and cell polarity, as a new scaffold of electrical

synapses. Interestingly, Sipa1l3 was able to interact with ZO-1, ZO-2 and Cx36, suggesting a pivotal role in electrical synapse function. In summary, our study provides the first detailed view of the electrical synapse proteome in retinal neurons, which is likely to apply to electrical synapses elsewhere.

Introduction

With the discovery of acetylcholine as the first neurotransmitter at the beginning of the 20th century, it was widely accepted that chemical synaptic transmission is the only means of communication for neurons. Decades later, several authors independently demonstrated evidence for the existence of electrical synapses in invertebrates as well as in vertebrates, and subsequent studies identified gap junctions, which are composed of clusters of intercellular channels, as the morphological substrates of these synapses (1, 2). Today it is considered common knowledge among neuroscientists that both types of synapses coexist in the nervous system and that each of them provides unique features essential for accurate signal processing. Yet, compared to the efforts that have been made to study protein complexes underlying chemical synapse function and regulation, we know fairly little about the proteome that constitutes an electrical synapse (3).

In contrast to chemical synapses, electrical synapses don't rely on neurotransmitters and specific receptor molecules but instead make use of intercellular channels to convey neural signals bidirectionally in the form of ionic currents (4). This seemingly simple mode of communication allows for an instantaneous signal transmission that synchronizes the activities of electrically coupled neurons giving rise to complex brain functions such as network oscillation, hormone secretion or coordination of motor functions (5, 6).

In the mammalian nervous system, electrical synapses are mainly, but not exclusively formed by Connexin 36 (Cx36), a connexin isoform that is highly specific for neurons (7-9) and often referred to as the "major neuronal connexin". One exception to the rule are the insulin producing beta cells in the pancreas (10). In general, Cx36 gap junction channels are known to exhibit a very low single channel conductance (11) but a remarkable degree of plasticity that allows neurons to regulate the number of open channels and hence the strength of synaptic transmission in order to adapt to environmental stimuli (12). A prime example of a neuron that is heavily coupled via Cx36 and in which the signal transduction pathways that regulate electrical coupling have been well described is the AII amacrine cell (13-15). The AII cell is a glycinergic interneuron in the mammalian retina that is electrically coupled to neighboring AII amacrine cells and to ON Cone

77 bipolar cells (16). The main task of this cell is to collect neural signals that originate in rods and
78 relay them into the cone pathway. This circuit is referred to as the primary rod pathway and it
79 forms the neurophysiological basis for scotopic vision. Within the primary rod pathway, electrical
80 coupling of AII amacrine cells is regulated in an activity dependent manner (13). The opening of
81 Cx36 channels in AII amacrine cells requires the activation of calcium calmodulin dependent
82 kinase II (CaMKII), which is triggered by the influx of calcium through non-synaptic NMDA
83 receptors. Once CaMKII is activated, it binds to Cx36 and phosphorylates the intracellular
84 domains causing the channel to open (13, 17, 18). These activity driven changes clearly resemble
85 long-term potentiation as it has been described for chemical synapses in hippocampal neurons
86 (19). Another, almost obvious, but not less important, parallel between electrical and chemical
87 synapses, is the their basic "architecture": 1) Glutamate receptors, for instance, interact with
88 PSD95 (20), a membrane associated guanylate kinase (MAGUK) that is similar in function and
89 domain structure to ZO-1, another MAGUK and well-known interactor of Cx36. 2) Electrical
90 synapses are surrounded by adhesions (21). 3) As described for glutamatergic synapses,
91 electrical synapses also harbor electron dense structures that appear to consist of a dense
92 assemblage of synaptic proteins (22, 23). However, the composition of this density or the type of
93 adhesion molecule that is necessary to specify where an electrical synapse is formed still remain
94 a mystery and require sophisticated proteomics to solve.
95
96 The task of identifying compartment specific proteomes or interactomes for a given protein of
97 interest (POI) with standard techniques has always been challenging due to the abundance of
98 non-specific background and the requirement to preserve intact protein complexes. To overcome
99 these limitations, several laboratories have developed novel proximity techniques such as
100 TurboID (24, 25), which utilize promiscuous biotin ligases to biotinylate neighboring proteins within
101 a radius of 5 nm of the POI. Like any other tag, TurboID can be fused to the POI and is then
102 expressed in cells, where it is allowed to biotinylate proximal proteins that are subsequently
103 isolated with streptavidin beads under stringent buffer conditions. The ability to directly label
104 "associated" proteins with an affinity tag combined with the fast enzyme kinetics have made
105 TurboID a valuable tool for modern *in vivo* proteomics. Previously, BioID and TurboID have been
106 used to study the proteomes of chemical synapses and even contact sites of astrocytes and
107 neurons in nematodes and mice (26-28).
108
109 In the present study, we have applied two different TurboID approaches to uncover the electrical
110 synapse proteome in the mouse and the zebrafish retina. Contrasting these two model organisms

111 allowed us to expose essential components of the molecular architecture of vertebrate electrical
112 synapses. Beyond known components of electrical synapses, such as ZO-1 and ZO-2, our screen
113 identified a plethora of new molecules that were not previously shown to associate with
114 Cx36/Cx35b. These include components of the endocytic machinery, adhesion molecules,
115 regulators of the cytoskeleton, membrane trafficking, as well chemical synapse proteins. Overall,
116 our screen showed that many components of electrical synapses in zebrafish and mouse retinas
117 were highly conserved, in particular the ZO proteins and the endocytosis components, indicating
118 a high degree of evolutionary conservation that suggests a critical functional role for these
119 proteins.
120

121 **Results**

122

123 **Two TurboID approaches allow a glimpse at the electrical synapse proteome in zebrafish**
124 **photoreceptors and AII amacrine cells of the mouse retina.**

125

126 In this study, we have adopted two *in vivo* BioID approaches to gain a more comprehensive
127 understanding of protein complexes that are associated with the neuronal connexin Cx36 and its
128 zebrafish orthologue Cx35b in retinal neurons. To implement BioID in zebrafish, we generated a
129 transgenic line expressing a Cx35b-V5-TurboID fusion protein (we used an internal insertion site
130 as previously described (29)) under the control of Cx35b promoter (Figure 1 A). As shown in
131 control experiments, the expression of this construct recapitulated the expression pattern of
132 wildtype Cx35b in photoreceptors (30) which were labelled with ZPR1, indicating that Cx35b-V5-
133 TurboID is correctly targeted to synapses (Figure 1B). The inner retina, however, displayed much
134 weaker expression of the fusion construct, which is why we anticipated that most of the candidates
135 we detected with this strategy are proteins that are associated with Cx35b in photoreceptors. To
136 induce efficient biotinylation in zebrafish we injected 10mM biotin solution intraperitoneally on
137 three consecutive days and isolated biotinylated proteins for mass spectrometry (Figure 1B and
138 C). A complete list of proteins captured in two experiments is shown in Supplement 1. For the
139 analysis of mass spec data sets we compared the abundance of candidate proteins from the
140 Cx35b-V5-TurboID strain to wildtype samples that did not express TurboID, and evaluated
141 specificity using Significance Analysis of Interactome (SAINT) (31). In Cx35b-V5-TurboID
142 samples, but not in wild type retinas, we found several known interactors of the Gjd2 family such
143 as scaffold proteins including Tjp1a, Tjp1b, Tjp2a, Tjp2b, Mupp1, Psd95 and Af6 (Figure 1D) (32-
144 35). In addition to these candidates, we identified proteins that are involved in membrane

145 trafficking including Syt4, Sec22b, components of the endosomal trafficking machinery Snap91
146 and Eps15l1a, and an additional Cx36 orthologue termed Cx34.7, which has previously been
147 localized to photoreceptors in bass retina (36). The detection of this Gjd1 isoform via BioID was
148 somewhat surprising, as Cx34.7 was shown to form gap junctions that are separated from Cx35b
149 containing clusters in bass photoreceptors. To determine the subcellular localization of Cx34.7
150 and its connection to Cx35b in zebrafish photoreceptors, we generated a transgenic Cx34.7-GFP
151 strain, that expressed an internally GFP-tagged fusion protein under the control of the Cx34.7
152 promoter. In this strain, we found that Cx34.7 was only expressed in the outer plexiform layer
153 (OPL) where it was associated with Cx35b at some gap junctions (Figure 1E). Thus, besides
154 known interactors of the Gjd family, our *in vivo* BioID approach identified an additional connexin
155 isoform that is connected to Cx35b in photoreceptors.
156
157 To unravel the Cx36 interactome in the mouse retina we initially delivered a Cx36-V5-TurboID
158 fusion via intravitreal AAV injections into retinal neurons. This construct was similarly designed to
159 the Cx35b clone but regulated by a short human synapsin promoter to drive expression in the
160 neural retina (Figure 2A). Unfortunately, this strategy produced massive overexpression artefacts
161 and resulted in an accumulation of Cx36-V5-TurboID in ganglion cell somas, which would have
162 made an interactome analysis of a synaptic protein impossible. To solve this issue and to ensure
163 that TurboID is targeting electrical synapses, we took advantage of the GFP-directed TurboID
164 approach (37) and the Cx36-EGFP transgenic mouse strain (38-40). The GFP-directed TurboID
165 strategy was initially developed as a modular system for zebrafish by Xiong et al., and utilizes and
166 a destabilized GFP nanobody that is fused to TurboID (37) to direct the biotin ligase towards a
167 given protein of interest carrying a GFP-Tag. To further increase the specificity of our approach
168 and identify the Cx36 interactome within a single type of inhibitory interneuron, the AII amacrine
169 cell, we expressed V5-TurboID-dGBP under control of the HKamac promoter (41). As shown
170 previously, in retinas that were infected with AAVs carrying an HKamac GFP vector, we observed
171 GFP expression mainly in AII amacrine cells but not in bipolar cells (Figure 2B, lack of GFP
172 expression in SCGN labelled neurons). In our hands, we also observed GFP labeling in horizontal
173 cells, which was neglectable for our paradigm, since these neurons do not express Cx36 (42) and
174 because dGBP is degraded unless it is bound to GFP (43). In an initial experiment we injected
175 AAVs carrying HKamac_V5-TurboID-dGBP intravitreally into Cx36-EGFP mice and tracked the
176 localization of the construct two weeks post injection. As expected, all V5 labeled puncta
177 colocalized with Cx36-EGFP, indicating that V5-TurboID-dGBP reached electrical synapses in AII
178 amacrine cells. In the next experiment, we injected a 5 mM biotin solution subcutaneously on 4

179 consecutive days, 3 1/2 weeks post infection. This treatment was sufficient to induce efficient
180 biotinylation (Figure 2B, lower panel and C) and allowed us to capture a plethora of molecules
181 that were associated with Cx36. To distinguish these proteins from background, we included wild
182 type mice injected with AAV HKamac_V5-TurboID-dGBP throughout the entire experiment. A
183 complete list of proteins captured in two experiments is shown in Supplement 2. We compared
184 the abundance of all proteins we detected and evaluated specificity using SAINT. A mass spec hit
185 that was three times or even more abundant in the Cx36-EGFP condition and with a SAINT score
186 greater than 0.5 was considered a candidate that is likely to be associated with Cx36. We
187 illustrated the relationship of all proteins that fell into this category in a string diagram (Figure 2D).
188 Among the most abundant proteins in our screen, we identified the ZO proteins ZO-1 and ZO-2
189 and signal induced proliferation associated 1 like 3 (Sipa1l3), a PDZ domain containing protein
190 that has been implicated in the regulation of cell adhesion and cell polarity. In addition to these
191 candidates, we also identified proteins that are involved in endocytosis, membrane trafficking,
192 regulation of the cytoskeleton, cell adhesion and chemical synapses. All of these hits covered
193 different functional categories of proteins that have been related to connexins (44-49) and thus
194 appear to represent an authentic interactome for a neuronal gap junction protein.
195
196 **Localization of BioID hits at Cx36 containing gap junctions in the AII amacrine cell**
197
198 In the next set of experiments, we validated the most abundant candidates from our list in GFP
199 expressing AII amacrine cells. We categorized the proteins based on the cell biological function
200 they serve. In line with the mass spec data, we observed the most frequent colocalization for
201 Cx36 with scaffold proteins including ZO-1, ZO-2, cingulin and Sipa1l3 (Figure 3A, arrows).
202 Although ZO-1, ZO-2 and cingulin are known components of electrical synapses (35, 45), Sipa1l3
203 has not been shown before to associate with Cx36, yet it colocalized with the connexin to a similar
204 extent as the ZO proteins, suggesting that it could be essential for synapse formation or
205 stabilization. In addition to scaffolding proteins, we confirmed an association with several adapter
206 proteins of the endocytic machinery, including Eps15l1, Snap91, Hip1r and Itsn1 (Figure 3B,
207 arrows). In comparison to the scaffold proteins, however, the colocalization of Cx36 with each of
208 these endocytic components was clearly less frequent and more heterogenous, which appears to
209 reflect different stages in the life cycle of Cx36. As most proteins we identified in this initial screen
210 broadly labeled the entire inner plexiform layer (IPL – the inner synaptic layer of the retina), we
211 performed a colocalization analysis to exclude a random overlap with Cx36. We quantified the
212 number of Cx36 plaques that contained Cgn, Sipa1l3, Eps15l1 and Hip1r (Figure 3C & D) and

213 compared the extent of colocalization to a control in which we flipped the Cx36 channel
214 horizontally. For each candidate, we found a significant reduction in colocalization, when the
215 original images were compared to the flipped control, indicating that the proteins we have
216 identified are actual components of electrical synapses.
217
218 Besides synaptic scaffolds and endocytic adapter proteins we tested a variety of additional hits,
219 which include synaptojanin 2 binding protein (Sj2bp), synaptotagmin 4 (Syt4; categorized as
220 "trafficking") and several proteins that regulate actin dynamics such as G-protein regulated
221 inducer of neurite outgrowth 1 (Gprin1), dedicator of cytokinesis 7 (Dock7) and microtubule
222 associated protein 6 (Map6). All of these proteins showed considerable colocalization with Cx36
223 in AII amacrine cell dendrites (Figure 4A, B). We also tested components of chemical synapses
224 including GluR2-3, the scaffold Shank2 (Figure 4D) and Bai1 (Figure 4C) a synaptic adhesion
225 molecule implicated in excitatory synapse formation (50). We found that these proteins showed a
226 partial overlap with Cx36 at the periphery of each junction. In addition to the candidates described
227 here, we identified additional candidates that were associated with Cx36 in AII amacrine cells
228 (supplemental figure 1-4). These include Ajm1 (Apical junction component 1), Cap1 (Adenylyl
229 cyclase associated protein1), Neurobeachin (Nbea), Ncam1 (Neural cell adhesion molecule 1),
230 Rtn4 (Reticulon4), Af6 (Afadin), Trim9 (Tripartite motif containing protein 9), Golga4 (Golgin
231 subfamily A member 4), Stxbp1 (Syntaxin binding protein 1) and Sipa1l1 (Signal-induced
232 proliferation-associated 1-like protein 1) (Supplementary figures 1-5).
233
234 **Identification of novel Cx36 binding partners**
235
236 Thus far, we have gained significant insight into the Cx36 interactome and identified several new
237 molecules as components of electrical synapses in AII amacrine cells. To understand how these
238 molecules are organized at the synapse we tested protein-protein interactions in co-transfected
239 HEK293T cells. Interestingly, two of the novel proteins we detected in AII cells contain PDZ
240 domains and thus may directly bind to Cx36 like ZO-1 and ZO-2 (Figure 5B, GFP-Trap IP with
241 both ZO proteins served as a positive control); these proteins are Sipa1l3 and Sj2bp. We found
242 that Myc-Sipa1l3 interacted with all major components of electrical synapses: ZO-1, ZO-2 and
243 Cx36 in co-transfected HEK293T cells. The overlap of Sipa1l3 and the ZO proteins was confined
244 to cell cortices and to actin like fibers in the cytoplasm (Figure 5A). Additionally, we performed IP
245 experiments and demonstrated that Cx36 binds to Sipa1l3 in a PDZ dependent manner. A
246 truncated version of Cx36 lacking the PDZ binding motif (Cx36/S318Ter) failed to interact with

247 Sipa1l3 in IP experiments. In co-transfected cells we observed that Sj2bp, which contains a single
248 PDZ domain and a transmembrane domain (51), colocalized with Cx36 but not with the
249 Cx36/S318Ter, indicating that the interaction of these proteins requires the PDZ domain. In IP
250 experiments using FLAG tagged Sj2bp as a bait we were unable to coprecipitate Cx36, which
251 was rather surprising as both proteins clearly colocalized in co-transfected HEK293T cells. One
252 possible explanation for the lack of a detectable interaction, is that Sj2bp displays a low affinity
253 for the PDZ binding motif (PBM) of Cx36, as it is the case for ZO-1 (46). We have previously
254 shown that binding of Cx36 to ZO-1 can be artificially enhanced by a simple deletion of amino
255 acids 313-319 within the C-terminus creating a new PBM with the following sequence: RTYV (52).
256 We repeated the IP with this mutant and observed substantial binding to FLAG-Sj2bp (Figure 5B),
257 suggesting that Cx36 and SJ2BP are compatible interactors. In addition to the candidates we
258 overexpressed to verify direct binding interactions, we found that Cx36 colocalized with several
259 endogenous HEK293T proteins that also occurred in our AII cell specific data set, including
260 Eps15l1, Gprin1 and Sec22b (Figure 5C).
261
262 **Molecular architecture of the AII amacrine cell/On cone bipolar cell gap junction.**
263
264 AII amacrine cells form two different sets of gap junctions, with neighboring AII amacrine cells and
265 with ON cone bipolar cells to convey neural signals that originate in rod photoceptors into the
266 cone pathway (Illustrated in figure 6A) (9). Ultrastructural studies have revealed an asymmetry in
267 the cytoplasm of AII/ON cone bipolar cell junctions (AII/ONCBC), which exhibits an electron dense
268 structure (termed fluffy material) in the AII amacrine cell but not in the cone bipolar cell, hinting at
269 differences in the molecular composition of both sites of the synapse (23, 53). Moreover, apart
270 from accessory proteins that bind to the channel, AII/ONCBC gap junctions are likely to be distinct
271 from AII/AII gap junctions since they recognize ON cone bipolar cells as the correct synaptic
272 partner. These two characteristics of the AII/ONCBC gap junction can only be explained by a
273 unique composition of the synapse proteome. We reasoned that the electron density in the AII
274 cell could harbor several proteins we identified in this study. To test this hypothesis, we triple
275 labelled AAV/HKamac_GFP infected retinas with Scgn, Cx36 and the main candidates from our
276 screen. With this strategy it was possible for us to visualize AII/ONCBC contacts (Figure 6 D,
277 arrows) and the precise localization of each candidate. To illustrate the localization of AII/ONCBC
278 gap junctions in a comprehensive way, we reconstructed the morphology of AII amacrine cells
279 using serial section transmission EM imaging. As seen in figure 6B, most AII/ONCBC gap

280 junctions (shown in yellow) were located above homologous AII/AII contacts (Cyan) and contained
281 electron densities on both sides (Figure 6C).
282
283 The scaffold proteins ZO-1, ZO-2, Cgn and Sipa1l3 localized at AII/ONCBC contacts suggesting
284 that they are a part of the electron density in AII cells (Figure 6D, arrows). In addition to these
285 proteins, we also confirmed that AII/Cone bipolar cell gap junctions contained Syt4, Eps15l1,
286 Sj2bp and Gprin1. Finally, we addressed the exact localization of the G protein coupled adhesion
287 receptor Bai1, a synaptic adhesion molecule that has been implicated in excitatory synapse
288 formation (50). Interestingly, we observed Bai1 at AII/ONCBC contacts, in the vicinity of Cx36,
289 which is consistent with the notion of synaptic adhesion molecules as an integral part of electrical
290 synapses (21, 54). This finding further implies that Bai1 might play a role in the formation of
291 AII/ONCBC contacts. However, further knock-out studies will be necessary to address the
292 concrete function of this adhesion molecule. Finally, we addressed the subcellular distribution of
293 Sipa1l3 at AII/ONBC gap junctions. We noticed that these junctions often displayed a ring like
294 shape, that contained Sipa1l3 in the center of each ring (Figure 6E). One possible interpretation
295 of this distinct sub-synaptic distribution is that Sipa1l3 is interacting with a type of adhesion
296 molecule that is directly adjacent to the gap junction.
297
298 **Electrical synapse scaffolds are targeted to AII amacrine cell/ ON cone bipolar cell contacts**
299 **in the absence of Cx36.**
300
301 Previous studies have shown that ZO-1 localizes to neuronal contact sites even in the absence
302 of connexins (34). This finding is consistent with a study by Meyer et al., (2014), who reported
303 that Cx36-EGFP containing gap junctions colocalize with ZO-1 at AII/ONCBC contacts despite a
304 C-terminal tag in the fusion protein that is known to interfere with PDZ domain mediated
305 interactions (39, 52). One possible interpretation of these observations is that ZO-1, a protein with
306 multiple protein-protein interaction domains, is connected to additional components of the gap
307 junction such as adhesion molecules, the actin skeleton or other MAGUKs that retain the scaffold
308 at the synapse. We wondered if a similar principle applies to the scaffold proteins that were
309 identified in this study and tested the localization of ZO-2 and Sipa1l3 in Cx36 KO retinas that
310 were infected with AAV/HKamac_GFP to visualize AII/ONCBC contacts. Here, we observed that
311 ZO-2 and Sipa1l3 showed a similar effect as ZO-1 and still localized to AII/ONCBC contacts in
312 Cx36 KO retinas (Figure 7A-C). Additionally, we quantified the density and size of immunoreactive
313 Sipa1l3 and ZO-1 in the inner plexiform layer of WT and Cx36 KO mouse retina (Figure 7D). While

314 the size of ZO-2 and Sipa1l3 puncta were unchanged in Cx36 KO mice, the density of both ZO-2
315 and Sipa1l3 puncta were reduced and the colocalization of ZO-2 and Sipa1l3 was reduced in
316 Cx36KO retina. Thus, loss of Cx36 resulted in a quantitative defect in formation of electrical
317 synapse density complexes.
318
319 **Discussion**
320
321 In the present study, we have used TurboID to uncover the electrical synapse proteome in retinal
322 neurons. Our screen identified a plethora of molecules that were associated with the neuronal
323 connexins Cx36/Cx35b in zebrafish and mice such as adhesion molecules, scaffold proteins,
324 chemical synapse proteins, components of the endocytic machinery and cytoskeleton associated
325 proteins (Illustrated in Figure 7 E-F). The presence of ZO proteins and endocytosis components
326 in the Cx36 and the Cx35b interactome data suggests a certain degree of conservation in the
327 proteome of electrical synapses (Supplementary Table 3). An apparent difference between
328 species, however, is the existence of additional ZO variants and Cx36 homologues in the
329 zebrafish genome (34), which are also represented in our Cx35b interactome. In contrast to the
330 bass retina, where it was shown that Cx35 and Cx34.7 form two distinct circuits (36), we found
331 that zebrafish photoreceptors formed gap junctions that contained both connexins. Cell culture
332 experiments have confirmed that Cx35 and Cx34.7 are able to form heterotypic channels (55)
333 that exhibit slightly altered voltage sensitivities compared to the homotypic channels. How exactly
334 these gap junction channels in zebrafish photoreceptors are configured and which exact cell types
335 they connect remains to be determined.
336
337 Among other proteins that were detected in this study, we identified Sipa1l3 as a novel scaffold
338 protein for electrical synapses. Interestingly, Sipa1l3 was also described as a component of post
339 synaptic densities of glutamatergic synapses in hippocampal neurons, and is known interact with
340 Fezzins, which occur in a complex with Shank3 (56). Additionally, we found that Sipa1l3 was able
341 to interact with Cx36 and the ZO proteins. This raises the question of what potential function
342 Sipa1l3 might serve given the abundance of colocalization with Cx36 in AII amacrine cells?
343 Genetic screens have shown that mutations in the Sipa1l3 gene result in abnormal eye and lens
344 development and a decrease in the formation of cell adhesions. Like other members of the Sipa1l
345 family, Sipa1l3 also contains a RAP GTPase activating protein (GAP) domain that is known to
346 regulate the activity of RAP proteins, which in the GTP-bound form impacts processes such as

347 adhesion and actin dynamics (57). One way in which Sipa1l3 might influence the formation of
348 electrical synapses might be as a regulator of Rap1 and its effector proteins. To determine the
349 exact function of Sipa1l3 further studies on KO mice will be required.
350
351 One striking aspect of the Cx36 interactome in AII amacrine cells is the abundance of the
352 endocytosis machinery. Considering the short half life time of Cx36 of 3.1 h (29) and the fact that
353 the turnover of electrical synapse proteins is a steady-state process (44), it makes sense that the
354 endocytic machinery is that well represented in our interactome data. Thus, besides
355 phosphorylation, it seems possible that the cellular regulation of turnover mechanisms could
356 function as an additional means to adjust the strength of electrical coupling between AII amacrine
357 cells.
358

359 **Is Bai1 necessary to form electrical synapses in the primary rod pathway?**

360 How and when it is determined where electrical synapses are formed is currently unknown. It has
361 been suggested that neuronal adhesion molecules serve as cues that wire the correct neurons
362 together (3). This task also has to be accomplished in the primary rod pathway, where AII
363 amacrine cells form synapses among each other and with ON Cone bipolar cells. Interestingly,
364 we identified the brain specific angiogenesis inhibitor 1 (Bai1) between AII amacrine and ON cone
365 bipolar cell gap junctions, which could suggest that Bai1 is necessary to connect these cells.
366 Recent reports have described Bai1 as a synaptogenic enzyme capable of regulating intracellular
367 signaling pathways that determine synapse formation. (50, 58). Thus, besides merely functioning
368 as a cell adhesion molecule, Bai1 might actively support synaptogenesis in AII amacrine cells at
369 a level that is hierarchical to Cx36 and its associated scaffolds, which would explain why these
370 cells form contacts with ON Cone bipolar cells even in the absence of Cx36.
371

372 **Cell type-specific differences in the Cx36 interactome?**

373 Our Cx36 interactome in AII amacrine cells showed no signs of the scaffold protein Mupp1,
374 although it was previously identified as component of electrical synapses in the retina and several
375 other brain regions (32). Interestingly, however, Mupp 1 was detected in our Cx35b interactome
376 in zebrafish retina. One feasible explanation is that AII cell gap junctions simply lack certain
377 scaffolds such as Mupp 1 that are used by electrical synapses of other neurons like bipolar cells,
378 which our approach did not consider. In general, it will be interesting to understand how well
379 certain components of the electrical synapse proteome are preserved between cell types.
380 Endocytosis and ZO proteins, for instance, are unlikely to be cell-type specific interactors of gap

junction channels and are more likely to be ubiquitous constituents of electrical synapses, given their critical function in the constant turnover of Cx36. This is also reflected in the evolutionary conservation of these components in the proteomes from zebrafish and mice. Bai1, on the other hand, a protein that is needed to establish specific synaptic contacts, may only occur in certain electrical synapses.

Material and Methods

Animal husbandry of zebrafish

Maintenance and breeding of zebrafish was conducted under standard conditions (59). Wild type (AB) zebrafish were purchased from the Zebrafish International Resource Center (ZIRC, Eugene, OR, USA). Fish were maintained on a 14 h light/10 h dark cycle. All procedures were performed in accordance with the ARVO statement on the use of animals in ophthalmic and vision research and US Public Health Service guidelines and have been reviewed and approved by the Institutional Animal Care and Use Committees at the University of Texas Health Science Center at Houston and the University of Houston.

Tol2 mediated transgenesis

Transgenic Cx35b-V5-TurboID fish were generated using the Tol2 system and a donor vector containing 4.5 kb of the Cx35b promoter, exon1 of the Cx35b gene and the open reading frame of Cx35-V5-TurboID. The coding sequence of V5-TurboID (25) was cloned into a region of the Cx35b gene encoding the C-terminal tail. V5-TurboID was inserted between leucine 285 and proline 286 to expose the 19 C-terminal amino acids of Cx35b. Additionally, the donor vector contained a Myl7 promoter driving mCherry expression in the heart to select larvae in which the construct was integrated into genome. Transgenic Cx34.7-oxGFP fish were generated in the same way using a donor vector containing 2.8 kb of the Cx34.7 promoter and the coding sequence of Cx34.7 with oxGFP inserted between aspartate 283 and methionine 284 in the C-terminus. To generate transgenic fish, the donor vector was co-injected with Tol2 transposase mRNA into embryos in the 1 cell stage as described previously (60). Transgenic individuals were raised to adulthood and mated.

414 **Animal Husbandry of mice**

415 The experiments in this study were conducted with wildtype mice (C57BL/6J), the Cx36-EGFP
416 strain (38-40) (Kindly provided by Dr. Hannah Monyer) and Cx36 Knock out mice (61) (Kindly
417 provided by Dr. David Paul). Animals of ages 2-12 months were used for experiments. All
418 procedures were performed in accordance with the ARVO statement on the use of animals in
419 ophthalmic and vision research and US Public Health Service guidelines and were approved by
420 the Institutional Animal Care and Use Committee at the University of Houston.

421

422 **AAV constructs and intravitreal injections**

423 All AAV constructs used in this study were generated with the pAAV-9-(5)-hSYN-CAMKII-GFP
424 vector kindly provided by Dr. Neal Waxham. The coding sequence of the AII amacrine cell specific
425 AII promoter Hkamac was previously described by Khabou et al., (2023), and synthesized as a
426 654 base pair gBlocks® fragment by IDT genomics. The hSYN promoter and the coding sequence
427 of CaMKII in the pAAV-9-(5)-hSYN-CAMKII-GFP vector were excised via XbaI and EcoRV and
428 the coding sequence of V5-TurboID-dGBP (37, 52, 62) and GFP were fused to the AII promoter
429 and integrated into the vector via Gibson assembly. Titers of AAV particles for different AAV
430 constructs varied ranging from $8x10^{12}$ to $1x10^{13}$ gc/ml. For each experimental condition similar
431 amounts of virus particles were injected. All virus particles were generated at the Baylor College
432 of Medicine gene vector core facility. All AAV vectors that were used in this study will be made
433 available via Addgene. Prior to each virus injection, mice were anesthetized with 3.5-3.9%
434 isoflurane using the SomnoSuite/Mouse STAT Pulse Oximeter (SS-01-03, Kent Scientific
435 Corporation). Once the animal was anesthetized, a small incision next to the pupil was made
436 using a 30 G needle. Afterwards, 1.5 µl of the virus solution was carefully injected intravitreally.
437 Eyes were collected 2-4 weeks after each experiment.

438

439 **DNA constructs**

440 FLAG-SJ2BP and Myc-SIPA1L3 constructs were used in previous studies (51, 63). Venus-ZO-1
441 (#56394) and GFP-ZO-2 (#27422) were purchased from Addgene. The FLAG-Gprin1 (Clone:
442 OMu09339D) and FLAG-EPS15L1 (Clone: OMu22488D) constructs were purchased from
443 Genscript. All Cx36 pcDNA3.1 expression vectors were generated in previous studies (52, 62,
444 64).

445

446

447 ***In vivo* Biotinylation**

448 *In vivo biotinylation in zebrafish.* Prior to biotin injections, adult zebrafish were anesthetized with
449 0.02% Tricaine and immobilized in a small wax mold. A small incision was made into the abdomen
450 and 30 µl of a 5mM biotin (solved in PBS) solution was injected intraperitoneally using a Hamilton
451 syringe. This procedure was repeated for 2 consecutive days. Afterwards the fish were sacrificed
452 by a cold shock and the retinas were extracted. The streptavidin pull down was carried out as
453 previously described (52, 62). 80 retinas for each condition (Wild type vs. Cx35b-V5-TurboID)
454 were used. The experiment was performed twice.

455 *In vivo biotinylation in mouse.* 3 ½ weeks after intravitreal virus injections mice were anesthetized
456 with isoflurane and 1ml of a 5mM biotin was injected subcutaneously for 4 consecutive days. 17
457 retinas of each condition (Cx36-EGFP vs. wild type) were used for the streptavidin pull down. The
458 experiment was performed twice.

459

460 **LC/MS/MS analysis**

461 For mass spectrometry analysis of streptavidin pull downs, samples were concentrated on a
462 acrylamide/bis-acrylamide stacking gel and processed via In-gel digestion. An aliquot of the tryptic
463 digest (in 2% acetonitrile/0.1% formic acid in water) was analyzed by LC/MS/MS on an Orbitrap
464 Fusion™ Tribrid™ mass spectrometer (Thermo Scientific™) interfaced with a Dionex UltiMate
465 3000 Binary RSLCnano System. Peptides were separated onto an analytical C18 column (100µm
466 ID x 25 cm, 5 µm, 18Å Reprosil-Pur C18-AQ beads from Dr Maisch, Ammerbuch-Entringen,
467 Germany) at flow rate of 350 nl/min. Gradient conditions were: 3%-22% B for 90 min; 22%-35%
468 B for 10min; 35%-90% B for 10 min; 90% B held for 10 min, (solvent A, 0.1 % formic acid in water;
469 solvent B, 0.1% formic acid in acetonitrile). The peptides were analyzed using data-dependent
470 acquisition method, Orbitrap Fusion was operated with measurement of FTMS1 at resolutions
471 120,000 FWHM, scan range 350-1500 m/z, AGC target 2E5, and maximum injection time of 50
472 ms; During a maximum 3 second cycle time, the ITMS2 spectra were collected at rapid scan rate
473 mode, with HCD NCE 34%, 1.6 m/z isolation window, AGC target 1E4, maximum injection time
474 of 35 ms . Dynamic exclusion was employed for 20 seconds.

475

476 **Data processing and analysis**

477 The raw data files were processed using Thermo Scientific™ Proteome Discoverer™ software
478 version 1.4. Spectra were searched against the Uniprot-Zebrafish or Uniprot-Mouse database
479 using Sequest. Search results were filtered to 1% FDR for strict conditions and 5% for relaxed
480 conditions using Percolator. Trypsin was set as the enzyme with maximum missed cleavages set

481 to 2. For peptide mapping. MS tolerance was set to 10 ppm, and MS/MS tolerance to 0.6 Da.
482 Carbamidomethylation of cysteine residues was used as a fixed modification, while oxidation of
483 methionine, N-terminal acetylation, and phosphorylation of serine and threonine were set as
484 variable modifications.
485

486 **Bioinformatics**

487 For both zebrafish and mouse, data from two experiments with matched experimental and control
488 samples were integrated into a single master table. A mean ratio of Cx35b/Cx36 conditions to the
489 control was used to identify proteins that were enriched greater than 3-fold. The data were also
490 analyzed using Significance Analysis of Interactome (SAINT) (31) implemented via the Resource
491 for Evaluation of Protein Interaction Networks (REPRINT), accessed at https://reprint-apms.org/.
492 Proteins exceeding the 3-fold enrichment threshold and a SAINT score greater than 0.5 were run
493 through the Cytoscape (V3.10.2) plugin ClueGo (V2.5.10) to identify the GO Biological Processes
494 that were upregulated in each Cx36 condition across both zebrafish and mouse species (65, 66).
495 Pathways that show a p-value of less than 0.05 were used for analysis. To determine protein-
496 protein interaction networks, proteins above threshold were also run through the standard
497 STRING (V12.0) pipeline (67).
498

499 **Cell culture**

500 Human embryonic kidney 293 T cells (HEK293T/17; catalog #CRL-11268; ATCC, Manassas, VA,
501 USA) were grown in Dulbecco's Modified Eagle Medium (DMEM) supplemented with 10% fetal
502 bovine serum (FBS), 1% penicillin and streptomycin, and 1% non-essential amino acids (all
503 Thermo Fisher Scientific, Rockford, IL, USA) at 37 °C in a humidified atmosphere with 5% CO2.
504 For pull-down experiments 1 million cells were plated in 60mm dishes. Transfections were carried
505 out with Geneporter 2 as previously described (52).
506

507 **Immunocytochemistry**

508 Immunolabeling of transfected HEK293T cells was carried out as previously described (62, 64).
509 Transfected HEK293T expressing the proteins of interest were briefly rinsed in PBS and fixed in
510 2% paraformaldehyde (PFA) solved in PBS for 15 min at RT. After the fixation step, the coverslips
511 were washed three times in PBS for 10 min and incubated with the primary antibody solution
512 containing 10% normal donkey serum in 0.5% Triton X-100 in PBS overnight at 4 ºC .The following
513 antibodies were used: mouse anti Cx36, 1:500 (MAB3045, Millipore), rabbit anti SIPA1l3, 1:200

514 (30544-1-AP, Proteintech), anti GFP, 1:250 (A10262, Thermofisher), rabbit anti EPS15L1, 1:250
515 (PA5-65940, Thermofisher) and mouse anti V5, 1:500 (R960-2, Thermofisher), rabbit anti Myc
516 (16286-1-AP, Proteintech). At the next day, the coverslips were washed 3x10 min in PBS and
517 incubated with the secondary antibodies diluted in 10% normal donkey serum in 0.5% Triton X-
518 100 in PBS at RT under light protected conditions. The following secondary antibodies were used:
519 from donkey, 1:500, conjugated with Cy3, Alexa488, Alexa568, or Alexa647 (Jackson
520 Immunoresearch, West Grove, PA). Afterwards coverslips were washed 3x10 min in PBS and
521 mounted with Vectashield containing DAPI (H-2000, Vector Laboratories Inc.)
522
523 **Immunohistochemistry**
524 Immunolabeling of vertical sections was carried out as previously described (68, 69). Mice were
525 anesthetized with isoflurane and sacrificed via cervical dislocation. The eyes were removed from
526 the animal and opened with a circular cut around the *ora serrata*. The lens was removed, eyes
527 were fixed with 2% PFA solved in PBS for 20 min at room temperature and washed 3x10 min in
528 PBS. Afterwards eyecups were stored in 30% sucrose at 4ºC overnight. On the next day eyecup
529 preparations were embedded in Tissue-Tek O.C.T. cryomatrix (Sakura Finetek, Torrance, CA,
530 USA) and stored at -20ºC. Eyecups were cut into 20 µm thin section and incubated at 37ºC for
531 30 min. Afterwards the slides were washed with PBS (2x5 min) and incubated in the primary
532 antibody solution containing 10% normal donkey serum in 0.5% Triton X-100 in PBS overnight.
533 The following primary antibodies were used: Cx36, 1:250 (Clone: 8F6, MAB3045, Millipore);
534 Cx36, 1:250 (Clone: 1E5H5, 37-4600, Thermofisher); GFP, 1:250 (A10262, Thermofisher); ZO-1,
535 1:250 (Clone: ZO1-1A12, 33-9100, Thermofisher); ZO-2, 1:250 (71-1400, Thermofisher); CGN,
536 1:250 (PA5-5561, Thermofisher); SIPA1L3, 1:100 (30544-1-AP, Proteintech); EPS15L1, 1:250
537 (PA5-65940, Thermofisher); HIPR1, 1:250 (AB9882,Sigma); GluR2-3, 1:200 (07-598, Sigma);
538 Gprin1, 1:100 (13771-1-AP, Proteintech); DOCK7, 1:100 (13000-1-AP, Proteintech); MAP6, 1:100
539 (NBP2-14220, Novus Biologicals); Synaptotagmin4, 1:100 (105 143, Synaptic Systems); SJ2BP,
540 1:100 (15666-1-AP, Proteintech); BAI1, 1:100 (NB110-81586, Novus Biologicals); SHANK2, 1:500
541 (Synaptic Systems, 162204); SCGN, 1:250 (CSB-PA020821LA01HU, ARP); SCGN, 1:500
542 (RD184120100, Biovendor); Vglut1, 1:500 (AB5905, Sigma); ITNS1, 1:100-250 (PA5-115432,
543 Thermofisher). The next day, the slides were washed 3x10 min and incubated with secondary
544 antibodies diluted in 10% normal donkey serum in 0.5% Triton X-100 in PBS for 1h at RT under
545 light protected conditions. The following secondary antibodies were used: from donkey, 1:250,
546 conjugated with Cy3, Alexa488, Alexa568, or Alexa647 or Dylight 405 (Jackson Immunoresearch,

547 West Grove, PA). Afterwards the slides were washed 3x10 min and mounted with Vectashield (H-
548 1900, Vector Laboratories, Inc.).
549
550 **Immunoprecipitation**
551 Immunoprecipitation experiments were carried out as previously described (47). 1.5 x10^6
552 HEK293T cells were plated on 60mm dishes and co-transfected at the next day with 2 µg of each
553 vector using Geneporter2 (Amsbio) transfection reagent. 24h after transfection, cells were rinsed
554 in phosphate buffered saline (pH 7.4) and transferred to a reaction tube. The cells were
555 centrifuged at 5000g for 5 min and afterwards homogenized in immunoprecipitation buffer (IP
556 buffer) containing 200mM NaCl, 2m EDTA, 1% Tx-100, 50mM Tris HCL (pH 7.5) supplemented
557 with protease inhibitors (Roche) and 1mM DTT. The lysate was sonicated 3x for 30 seconds and
558 incubated on ice for 30 min. Afterwards, the lysate was centrifuged at 10,000g for 10 min. 20 µl
559 of ChromoTek GFP-Trap® agarose beads (gta, Proteintech) were applied to the supernatant and
560 incubated overnight at 4ºC on a rotating platform. The next day the sample was centrifuged at
561 2500g for 5 min and washed three times in IP buffer. Bound proteins were eluted with 60 µl of 1x
562 Laemmli buffer (BioRad, 1610747) for 5 min at 95ºC. IP experiments for Myc-Sipa1l3 and FLAG-
563 Sj2bp were conducted under a slightly modified protocol. For IP experiments with Myc- Sipa1l3
564 0.5 µg of Sipa1l3 antibody (30544-1-AP, Proteintech) was applied to the cell lysate and incubated
565 overnight on a rotating platform. The next day, 40 µl of prewashed protein A/G beads (Pierce)
566 were applied to the cell lysate and incubated for 1h at 4 ºC. Afterwards the beads were washed 3
567 times and bound proteins were eluted with 1x Laemmli buffer. IP experiments with FLAG-Sj2bp
568 were performed with 20 µl ChromoTek DYDDDDK Fab-Trap® (ffa, Proteintech). Prior to the IP
569 cell lysates were centrifuged at 20,000g for 30 min at 4ºC. Afterwards, cell lysates were incubated
570 with agarose overnight and washed 3 times at 4ºC. Bound proteins were eluted with 60 µl of 1x
571 Laemmli buffer.
572
573 **Western blot**
574 Protein samples were separated via SDS-PAGE containing 7.5% (for Sipa1l3 blots) or 10%
575 polyacrylamide. Proteins were transferred to nitrocellulose membranes using the transblot turbo
576 system as previously described (52). Blots were blocked in 5% dried milk powder in TBST (20 mM
577 Tris pH 7.5, 150 mM NaCl, 0.2% Tween 20) for 30 min at RT and incubated overnight in the
578 primary antibodies diluted in blocking solution at 4ºC on a rotating platform. The following primary
579 antibodies were used: Cx36, 1:500 (Clone: 8F6, MAB3045, Millipore); Cx36, 1:500 (Clone:
580 1E5H5, 37-4600, Thermofisher), SIPA1L3, 1:4000 (30544-1-AP, Proteintech), GFP, 1:1000 (2956,

581 Cell Signaling), V5 1:1000 (R960-2, Thermofisher). Biotinylated proteins detected with high
582 sensitivity streptavidin-HRP, 1:1000 (Abcam). At the next day, blots were washed 3x10 min in
583 TBST and incubated with the secondary antibodies, diluted in the blocking solution as described
584 previously (52). The following secondary antibodies were used: goat anti mouse HRP, 1:1000
585 (34130) and goat anti rabbit, 1:1000 (34160, Thermofisher). Afterwards, the blots were washed
586 3x10 min in TBST and incubated with the ECL solution (32106, Thermofisher) for detection. ECL
587 was detected with the Biorad ChemicDoc™ MP Imaging System.
588

589 **Confocal microscopy and image analysis**

590 Fluorescence images were acquired with a confocal laser scanning microscope (Zeiss LSM 800)
591 using a 60x oil objective and the Airy scan function (Pixel size: 50 nm). Confocal scans were
592 processed using Fiji (ImageJ2 version 2.14.0/1.54f) software (70). The threshold was adjusted
593 using the *Triangle* function for the entire z-stack (7 slices; 1.08 µm). Two regions of interest (ROI)
594 with the size of 20.07 x 32.91 μm^2 were positioned to cover the ON and OFF IPL layers. Frequency
595 and size of the immunoreactive puncta were measured for each channel using the "analyze
596 particles" function. Colocalization of ZO-1 and Sipa1l3 was quantified using the *Colocalization*
597 plugin in Fiji. The number of colocalized puncta and the colocalization was measured using the
598 *Analyze* particle function with a size an exclusion criterion of $>100^2$ pixels. Following the
599 quantification, the size, density and percentage of the colocalized puncta were averaged for each
600 protein.
601

602 **Volume construction**

603 Retinal Connectome 2 (RC2) is an ultrastructural dataset acquired from the retina of a light-
604 adapted 5-month-old female C57BL/6J mouse (71). Methods concerning tissue acquisition and
605 processing, volume assembly, visualization, and annotation following that extensively detailed for
606 RC1 (72, 73). In short, the RC2 dataset spans the ganglion cell layer through outer nuclear layer
607 of a 0.25 mm-diameter field of retina. RC2 was constructed from 1335 serial TEM sections (70
608 nm thick), captured at 2.18 nm/pixel via Automated Transmission Electron Microscopy at 5000X
609 and combined with 31 optical sections intercalated throughout the volume. These optical sections
610 were probed for small-molecule signals for computational molecular phenotyping (74). Sections
611 were aligned into a single volume using the NCR ToolSet, which has since been replaced by
612 Nornir (RRID:SCR_016458). All protocols were in accord with Institutional Animal Care and Use
613 protocols of the University of Utah, the ARVO Statement for the Use of Animals in Ophthalmic

614 and Visual Research, and the Policies on the Use of Animals and Humans in Neuroscience
615 Research of the Society for Neuroscience.
616

617 **Statistical analysis**

618 Data sets acquired in this study were analyzed with GraphPad Prism 8. Data are shown as
619 mean ± SEM. Normality was tested using the Anderson–Darling and the D'Agostino-Pearson test.
620 Significance was tested using the two-tailed Mann–Whitney U test. For multiple comparisons a
621 one-way ANOVA was performed.
622

623 **Acknowledgements**

624 This project was supported by NIH grants R01EY012857 (J.O.), RF1MH120016 (A.E.P., J.O.),
625 and R21NS085772 (A.E.P., J.O.) and core grant P30EY007551. S.T. was funded by the *Deutsche*
626 *Forschungsgemeinschaft* (DFG) (TE 1459/1-1, Walter Benjamin stipend). E.S. was supported by
627 NIH training grant TL1TR003169 and individual grant F31EY034793. B.W.J. and C.L.S. are
628 supported by NIH grants R01EY028927 (to B.W.J.) and P30EY014800 (to the Moran Eye Center
629 Core); NSF grant 2014862; an Unrestricted Research Grant from Research to Prevent Blindness,
630 New York, NY to the Department of Ophthalmology & Visual Sciences, University of Utah; and an
631 Unrestricted Research Grant from Gabe Newell (to B.W.J.). This work is supported in part by the
632 Clinical and Translational Proteomics Service Center at the University of Texas Health Science
633 Center We would like to thank Li Li from the UT health mass spec. facility We would like to thank
634 Dr. Adam C. Miller and Dr. Jen Michel for the helpful discussions. We appreciate Nikki Brantley's
635 support in the cell culture lab.
636

637 **Author contributions**

638 S.T and J.O designed the research. S.T, E.S, E.O.A.M.K, H.H, F.A.E, C.L.S, Y.P.L and K.D
639 performed experiments. K.E and C.R contributed reagents and analytic tools. S.T wrote the paper.
640 All authors edited the paper.

641

642 **Figure legends**

643

644 **Figure 1: Generation of a Cx35b-V5-TurboID zebrafish line. (A)** Cartoon illustrating the
645 generation of Cx35-V5-TurboID fish via Tol2-mediated transgenesis and outline of *in vivo*
646 biotinylation experiments. To induce efficient proximity labeling, zebrafish were intraperitoneally

injected with 30µl of 5mM biotin (PBS) for three consecutive days. Afterwards the animals were sacrificed, and the retinas were isolated for streptavidin pull-downs. **(B)** Confocal scans of entire zebrafish retinas, the outer retina including ZPR1 labeled photoreceptors to confirm successful targeting of Cx35b-V5-TurboID to photoreceptor gap junctions. Neutravidin Oregon Green labeling was used to validate efficient proximity biotinylation of Cx35b and surrounding molecules in biotin injected Cx35b-V5-TurboID fish. Reagent or antibody used for labeling is shown in the gray box above each image. Scale 10µm. **(C)** Western blot of streptavidin pull-downs probed with V5 antibodies and streptavidin-HRP. The arrows indicate the position of the Cx35-V5-TurboID construct, which is detected with streptavidin-HRP and a V5 antibody. **(D)** String diagram illustrating the protein-protein network surrounding Cx35b. Proteins that were two times or more abundant in comparison to the control condition were included in the string diagram. **(E)** Colocalization of Cx35b and Cx34.7-GFP in the outer plexiform layer of the zebrafish retina suggests that a subset of photoreceptor gap junctions contain both connexins. Scale: 5 µm; inset scale: 0.5 µm.

Figure 2: A GFP-directed TurboID approach uncovers the Cx36 interactome in AII amacrine cells. (A) Cartoon illustrating different *in vivo* BioID approaches used to target Cx36. In strategy 1 we expressed an AAV Cx36-V5-TurboID construct with an internal insertion site under the control of the human synapsin promoter. This strategy greatly resulted in overexpression artefacts causing aberrant protein localization. In strategy 2 we adapted the GFP-directed TurboID strategy developed by Xiong et al., (37) to shuttle a V5-dGBP-TurboID construct to Cx36-EGFP containing gap junctions in retinas of the Cx36-EGFP transgenic strain. **(B)** Vertical sections of AAV infected retinas confirming cell type-specificity of our AAV vectors. The HKamac promoter developed by Khabou et al. (41) is mainly active in AII amacrine cells, and does not show any expression in bipolar cells (SCGN, magenta). V5-dGBP-TurboID colocalizes with Cx36-EGFP in AAV transduced retinas, confirming the successful delivery of TurboID to the gap junction. Scale: 5µm. **(C)** Western blot confirming successful biotinylation and capture of Cx36-EGFP, biotinylated proteins and V5-TurboID-dGBP. **(D)** String diagram illustrating the protein-protein interaction network associated with Cx36 in AII amacrine cells. Proteins that were three times or more abundant compared to the control condition were included in the string diagram.

Figure 3: Localization of scaffold and endocytosis proteins identified by BioID at Cx36 gap junctions in AAV transduced AII amacrine cells expressing GFP. (A) Colocalization of Cx36 and scaffold proteins including known interactors such as ZO-1, ZO-2 and cingulin. Besides these

681 known interactors, we identified Sipa1l3, a PDZ domain containing protein implicated in cell
682 adhesion and cytoskeletal organization. Sipa1l3 shows abundant colocalization with Cx36. **(B)**
683 Colocalization of Cx36 and components of the endocytosis machinery. Among all proteins we
684 have tested, we found frequent colocalization for EpsS15l1, an endocytic adapter protein, and
685 Cx36. Scale: 10 µm. Magnified inset: 1 µm. **(C)** Bar graphs showing the degree of colocalization
686 as the percentage of Cx36 puncta that overlap with Cgn and Sipa1l3. Colocalization was
687 quantified for the original image and a horizontally flipped image to exclude random overlap. Bar
688 graphs with SEM, $p < 0.05$ *** for Cx36 and Cgn and $p < 0.0001$ **** for Cx36 and Sipa1l3.
689 Significance for Cx36 and Cgn was determined using a Wilcoxon matched-pairs signed rank test.
690 Significance for Cx36 and Sipa1l3 was determined using a two-tailed paired t-test. **(D)** Bar graphs
691 showing the degree of colocalization as the percentage of Cx36 puncta that overlap with
692 endocytosis proteins the Ep15l1 and Hip1r. Bar graphs with SEM, $p < 0.0001$ **** for Cx36 and
693 Eps15l1 and $p < 0.05$ *** for Cx36 and Hip1r. Significance was determined using a two-tailed
694 paired t-test.
695
696 **Figure 4: Localization of trafficking, cytoskeleton-associated, adhesion and synaptic**
697 **proteins identified by BioID at Cx36 gap junctions in AAV transduced AII amacrine cells**
698 **expressing GFP. (A)** Proteins implicated in membrane trafficking Sj2bp and Syt4 colocalize with
699 Cx36 in AII amacrine cells. **(B)** Several cytoskeleton associated proteins and regulators such as
700 Map6, Dock7 or Gprin1 colocalize with Cx36 in AII cell dendrites. **(C)** The adhesion molecule Bai1
701 was often colocalized with Cx36 in AII cell dendrites. **(D)** Often components of chemical synapses
702 such as Shank2 and Glur2-3 were found in the periphery of gap junction plaques in AII amacrine
703 cells. Scale: 10 µm. Magnified inset: 1 µm.
704
705 **Figure 5: Sipa1l3, Sj2bp and Eps15l1 interact with Cx36. (A)** Coexpression of Sipa1l3 with
706 ZO-1, ZO-2 and Cx36. In transfected HEK293T cells Sipa1l3 colocalizes with all three proteins.
707 Colocalization of Sj2bp with Cx36 but not with a Cx36 mutant that lacks the PDZ binding motif.
708 **(B)** Domain organization of constructs used for IP experiments. Co-precipitation of Cx36 and
709 Sjbp2 and Sipa1l3 from lysates of co-transfected HEK293T cells. The PDZ binding deficient
710 Cx36/S318Ter fails to bind Sjbp2 and Sipa1l3. IP experiments with ZO-1 and ZO-2 serve as a
711 positive control. The proteins that were captured in each IP experiment are indicated with arrows
712 in magenta. Cx36 dimers in IP samples are indicated with red arrows and monomers are indicated
713 with blue arrows. **(C)** In transfected HEK293T cells, Cx36 is associated with endogenous proteins
714 that were also detected in AII amacrine cells. Line scans next to each panel illustrate the close

715 association of these proteins (57) with Cx36 (magenta). These proteins were also captured via
716 GFP directed proximity biotinylation. Scale: 10 µm. Magnified inset: 1µm.
717
718 **Figure 6: Localization of BioID "hits" at AII amacrine cell/ON cone bipolar cell junctions.**
719 **(A)** Cartoon illustrating the neurons involved in the primary rod pathway and the subcellular
720 localization of AII/Cone bipolar cell junctions (dashed rectangle). **(B)** 3D reconstruction of AII
721 amacrine cells from the RC2 connectomics dataset illustrating the localization of AII-AII gap
722 junctions (cyan plaques in second image) and AII/ON Cone bipolar cell gap junctions (yellow
723 plaques in second image). **(C)** EM micrographs of AII/ON Cone bipolar cell gap junctions. Pseudo
724 colored: Gap junction (Cyan), AII cell (Magenta) and ON cone bipolar cell (Yellow). White box
725 indicates area shown to right at 40000X magnification (0.27 nm/px resolution) with 20 degree tilt.
726 The density profile for the ROI indicated by the yellow box confirms the pentalaminar (dark-light-
727 dark-light-dark) structure of a gap junction. Also note the asymmetric cytoplasmic densities on the
728 AII versus ON Cone bipolar cell sides. Scale: 0.5 µm. **(D)** Several of the proteins we identified in
729 AII amacrine cells colocalize with Cx36 at AII/cone bipolar cell junctions. The right plot for each
730 panel depicts an intensity scan of a horizontal region of interest in the middle of each gap junction
731 (arrow). Scale: 10 µm. Magnified inset: 1 µm. **(E)** High resolution scan highlighting the subsynaptic
732 distribution of SIPA1L3. Scale: 5 µm. Magnified inset: 1 µm.
733
734
735 **Figure 7: AII amacrine cell/ON cone bipolar cell contacts remain in Cx36 KO retinas and**
736 **contain electrical synapse scaffolds. (A-C)** AII amacrine cell/ON cone bipolar cell contacts
737 were visualized with GFP and SCGN. In Cx36 KO retinas, ZO-1, ZO-2 and Sipa1l3 still localize
738 to AII/CBC contacts. **(D)** Both Sipa1l3 and ZO-1 puncta density in the inner plexiform layer were
739 reduced in Cx36KO, but puncta size was unchanged. Colocalization of Sipa1l3 and ZO-1 was
740 reduced in Cx36KO. **(E-F)** Cartoon illustrating Scale: 10 µm. Magnified inset: 1µm.
741
742 **Figure S1: Localization of additional proteins captured with BioID. (A)** Ajm1 labels the base
743 of AII cell somas but does not directly colocalize with Cx36. **(B)** Cap1 is associated with Cx36 in
744 AII cell dendrites. **(C)** Nbea does not directly associate with Cx36 but is often found close Cx36
745 clusters. Scale: 10 µm.
746

747 **Figure S2: Localization of Ncam1, AF6, Rtn4 and Trim9 cluster in proximity to Cx36 in the**
748 **inner retina. (A-B)** Ncam1 and Af6 labeling is found adjacent to Cx36 containing gap junctions
749 in the inner retina. **(C-D)** Rtn4 and Trim9 colocalize with Cx36 in the IPL. Scale**:** 10 µm.
750
751 **Figure S3: Localization of Golga4 in the somas of AII amacrine cells.** Golga4 labeling is
752 absent from the IPL and detected in the in INL including somas of AII amacrine cells. Scale: 10
753 µm**.**
754
755 **Figure S4: Partial colocalization of Cx36 and Stxbp1 in the IPL.** Stxbp1 labeling broadly
756 covers the entire IPL and colocalizes occasionally with Cx36. Scale: 10 µm.
757
758 **Figure S5: Colocalization of Cx36 and Sipa1l1 in the IPL. (A)** Colocalization of Cx36 and
759 Sipa1l1 puncta in arboreal dendrites of AII amacrine cells. **(B)** Additional example of Cx36/Sipa1l1
760 colocalization in the IPL. Scale: 10 µm.
761
762 **Figure S6**: Table showing a comparison of the most abundant proteins in the electrical synapse
763 proteomes of mice and zebrafish retinas. ZO proteins, Afadin and endocytosis proteins occur in
764 the electrical synapse proteomes of both species.
765

766 **Figures**

767 **Figure 1**

768

769 770 771 772 773 774 775 776 777 778 779 780 781 782 783 784 785 786 787 788 789

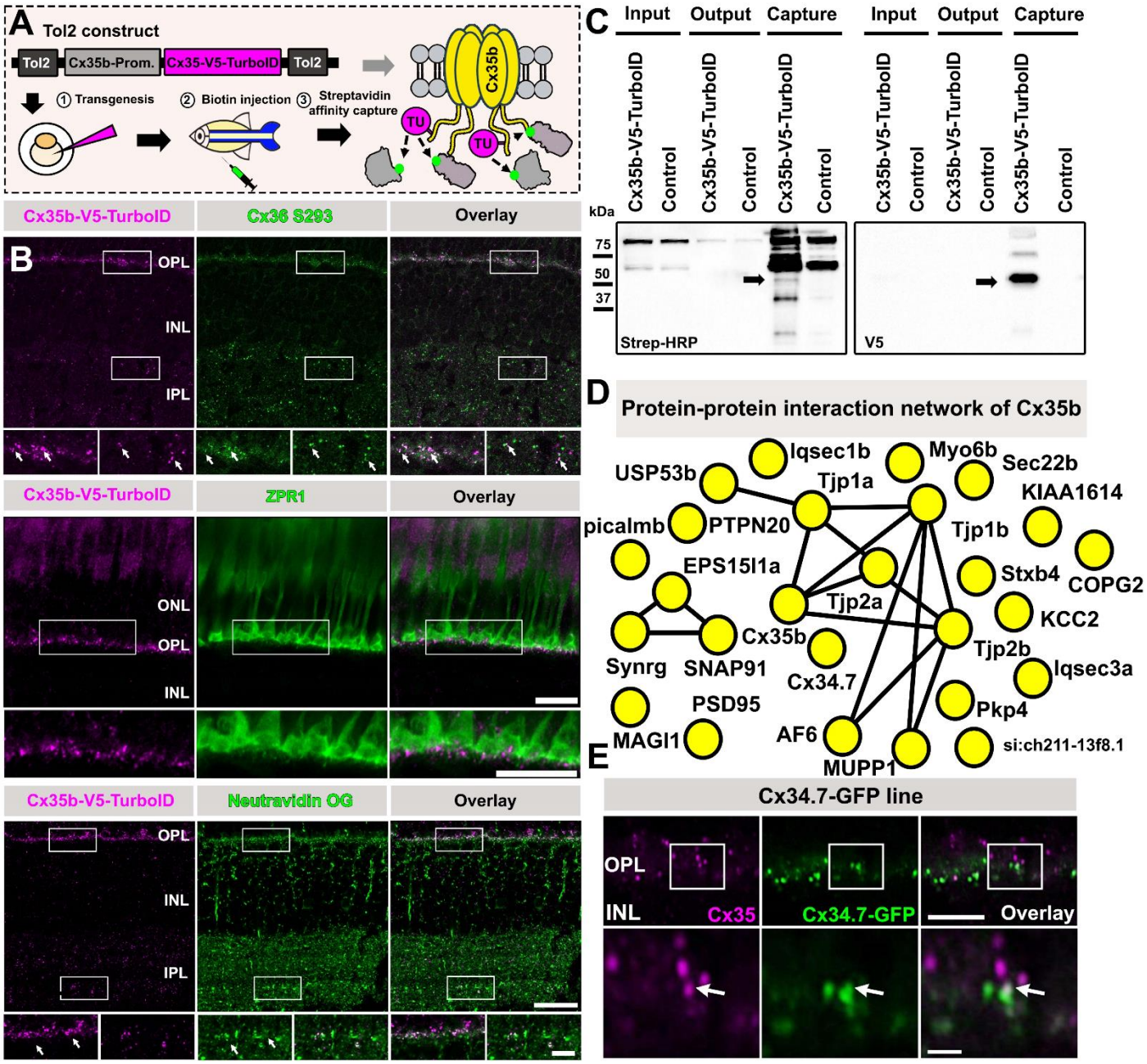

790

791

792

793

Figure 2

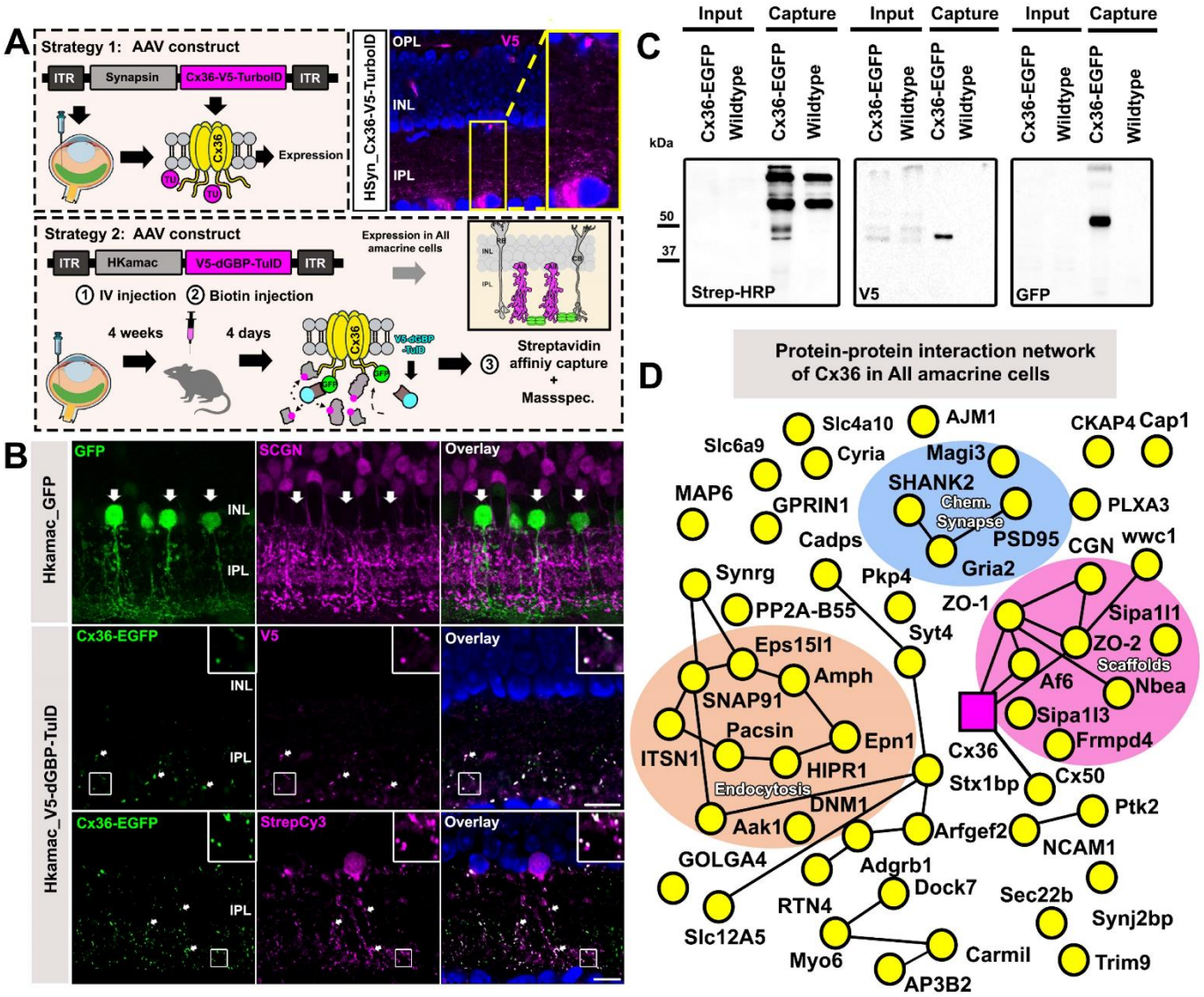
A
Strategy 1: AAV construct
ITR
Synapsin
Cx36-V5-TurboID
ITR
Cx36
TU
Expression
HSyn_Cx36-V5-TurboID
OPL
V5
INL
IPL
Strategy 2: AAV construct
ITR
HKamac
V5-dGBP-TuID
ITR
Expression in All amacrine cells
① IV injection ② Biotin injection
4 weeks
4 days
Cx36
V5-dGBP -TuID
GFP
③ Streptavidin affiniy capture + Massspec.
B
Hkamac_GFP
GFP
SCGN
Overlay
INL
IPL
Hkamac_V5-dGBP-TuID
Cx36-EGFP
V5
Overlay
Cx36-EGFP
StrepCy3
Overlay
C
Input
Capture
Cx36-EGFP
Wildtype
kDa
50
37
Strep-HRP
V5
GFP
D
Protein-protein interaction network of Cx36 in All amacrine cells
Slc4a10
AJM1
CKAP4
Cap1
Slc6a9
Cyria
Magi3
SHANK2
Chem. Synapse
PSD95
Gria2
MAP6
GPRIN1
Cadps
PLXA3
CGN
wwc1
Synrg
Pkp4
PP2A-B55
ZO-1
Sipa1l1
ZO-2
Scaffolds
Nbea
Af6
Sipa1l3
Frmpd4
Syt4
Eps15l1
Amph
SNAP91
Pacsin
Epn1
ITSN1
HIPR1
Endocytosis
Cx36
Stx1bp
Cx50
DNM1
Aak1
Arfgef2
Ptk2
NCAM1
GOLGA4
Adgrb1
Dock7
Sec22b
RTN4
Synj2bp
Slc12A5
Myo6
Carmil
Trim9
AP3B2

822 **Figure 3**

823

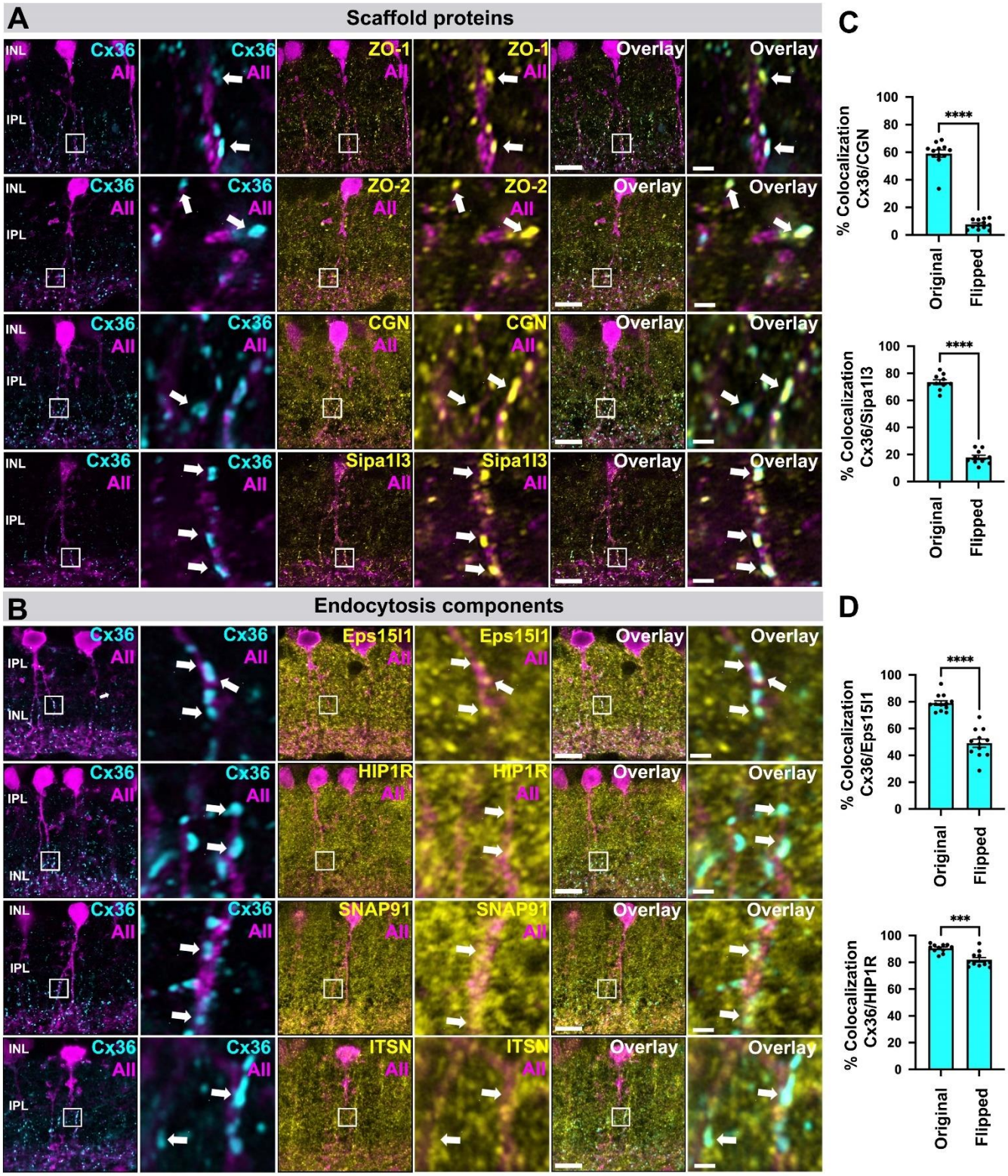

849

850 **Figure 4**

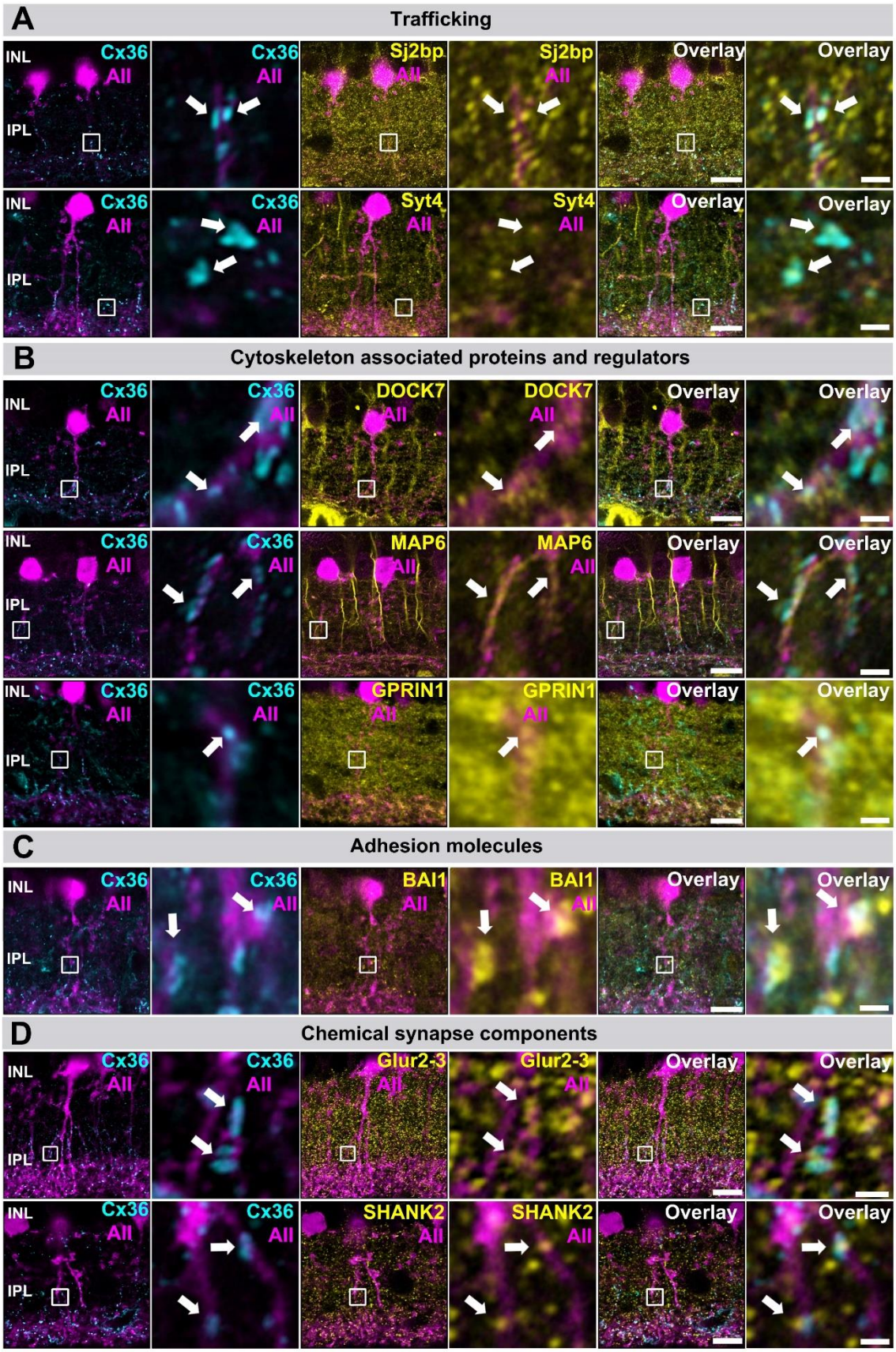
A
Trafficking
INL
IPL
Cx36
AII
Sj2bp
Syt4
Overlay
B
Cytoskeleton associated proteins and regulators
DOCK7
MAP6
GPRIN1
C
Adhesion molecules
BAI1
D
Chemical synapse components
Glur2-3
SHANK2

878 **Figure 5**

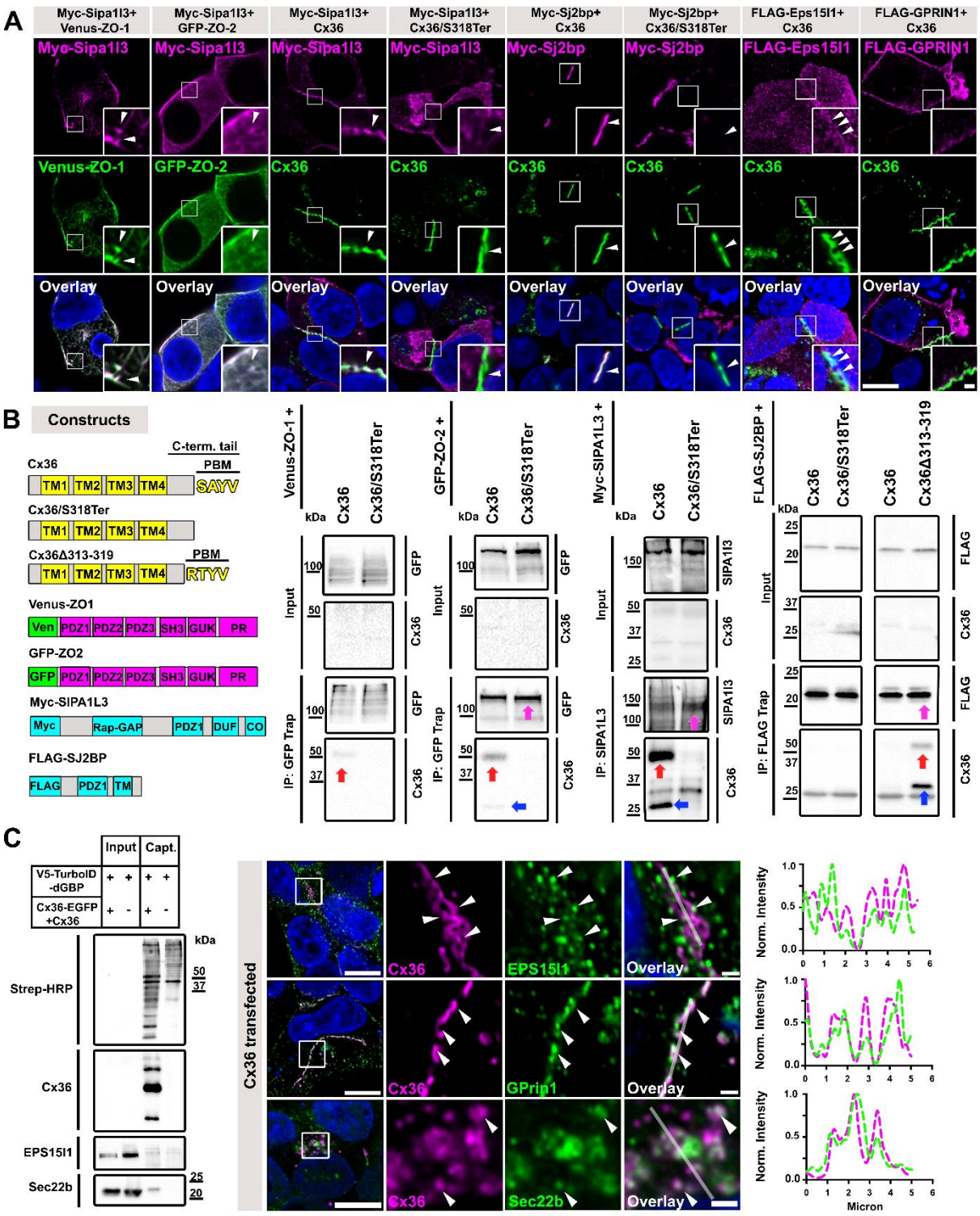

904

905

Figure 6

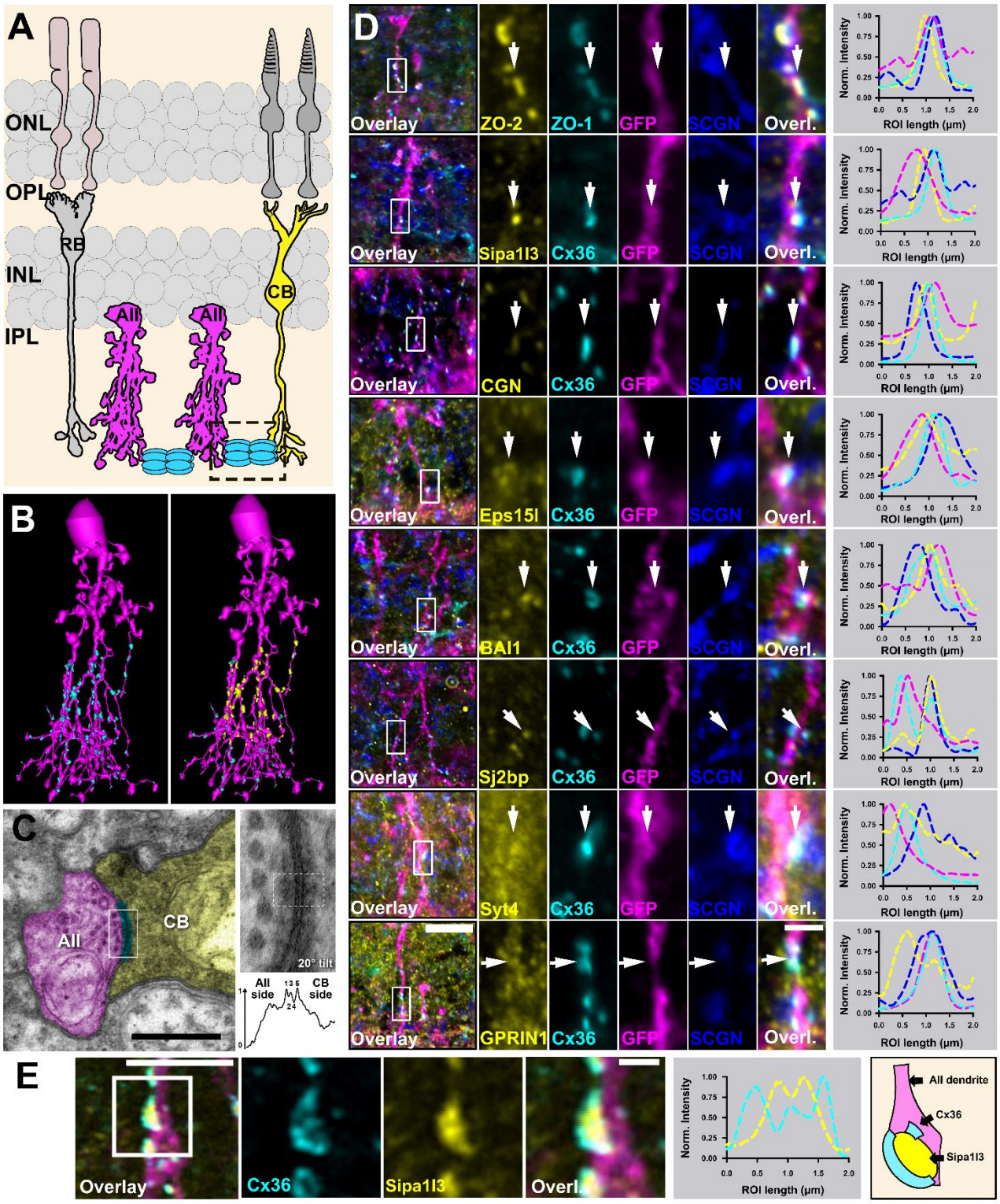
A
ONL
OPL
RB
INL
CB
AII
AII
IPL
B
C
AII
CB
20° tilt
AII side
CB side
D
Overlay
ZO-2
ZO-1
GFP
SCGN
Overl.
Sipa1l3
Cx36
CGN
Eps15l
BAI1
Sj2bp
Syt4
GPRIN1
Norm. Intensity
ROI length (µm)
E
Overlay
Cx36
Sipa1l3
Overl.
All dendrite
Cx36
Sipa1l3

934 **Figure 7**

935 936 937 938 939 940 941 942 943 944 945 946 947 948 949 950 951 952 953 954 955 956 957 958 959 960

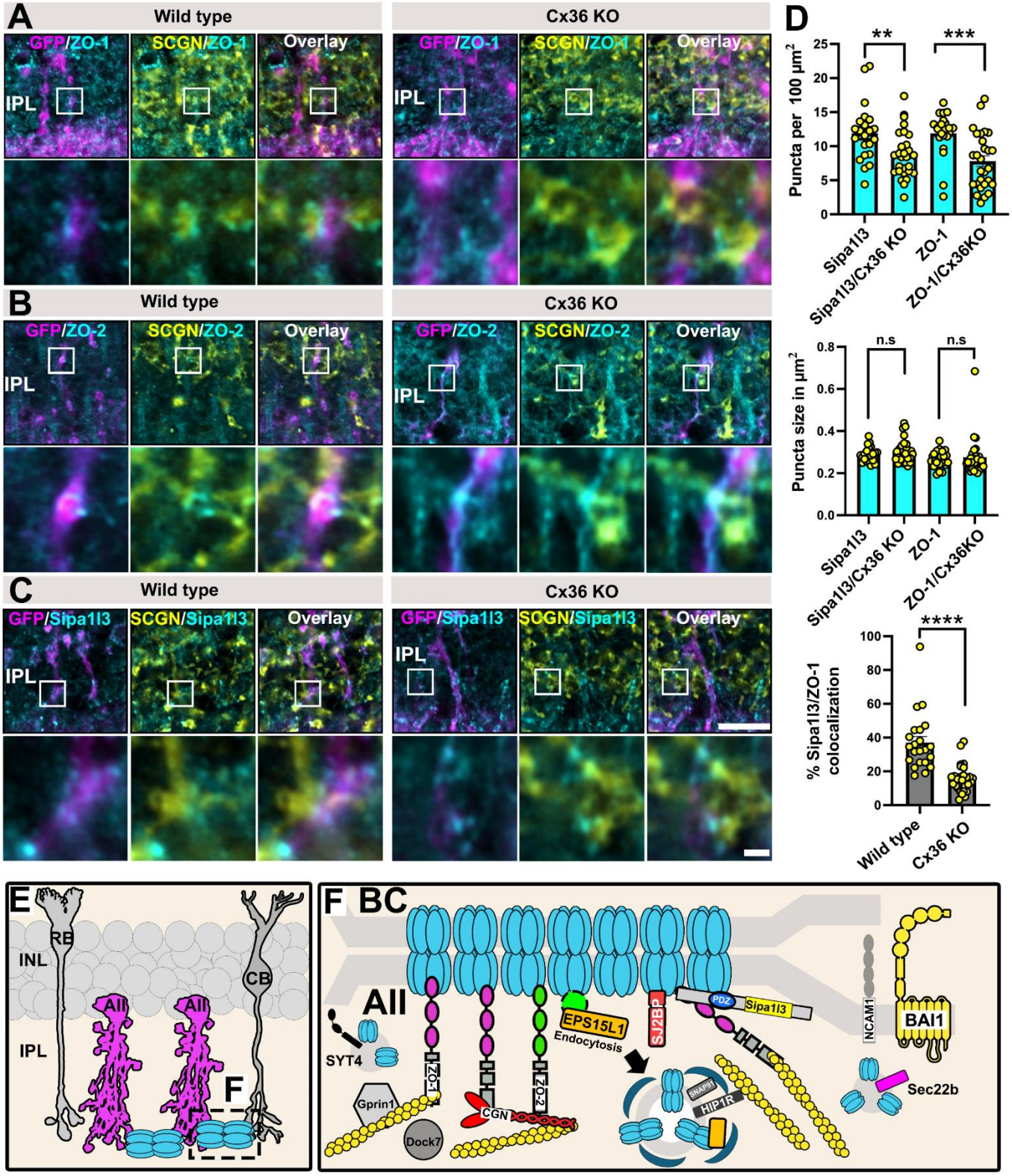

Supplementary figure 1

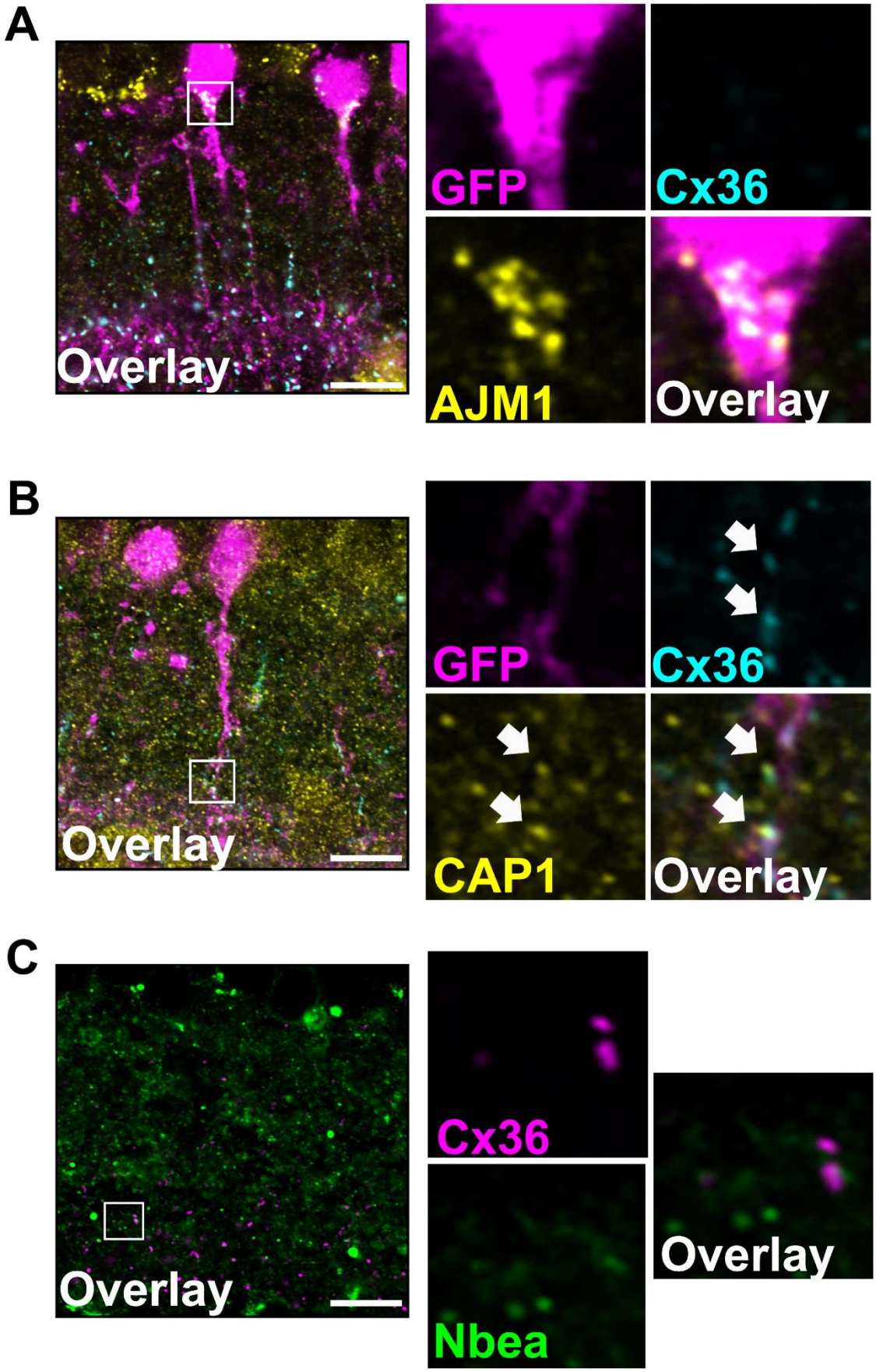

Supplementary figure 2

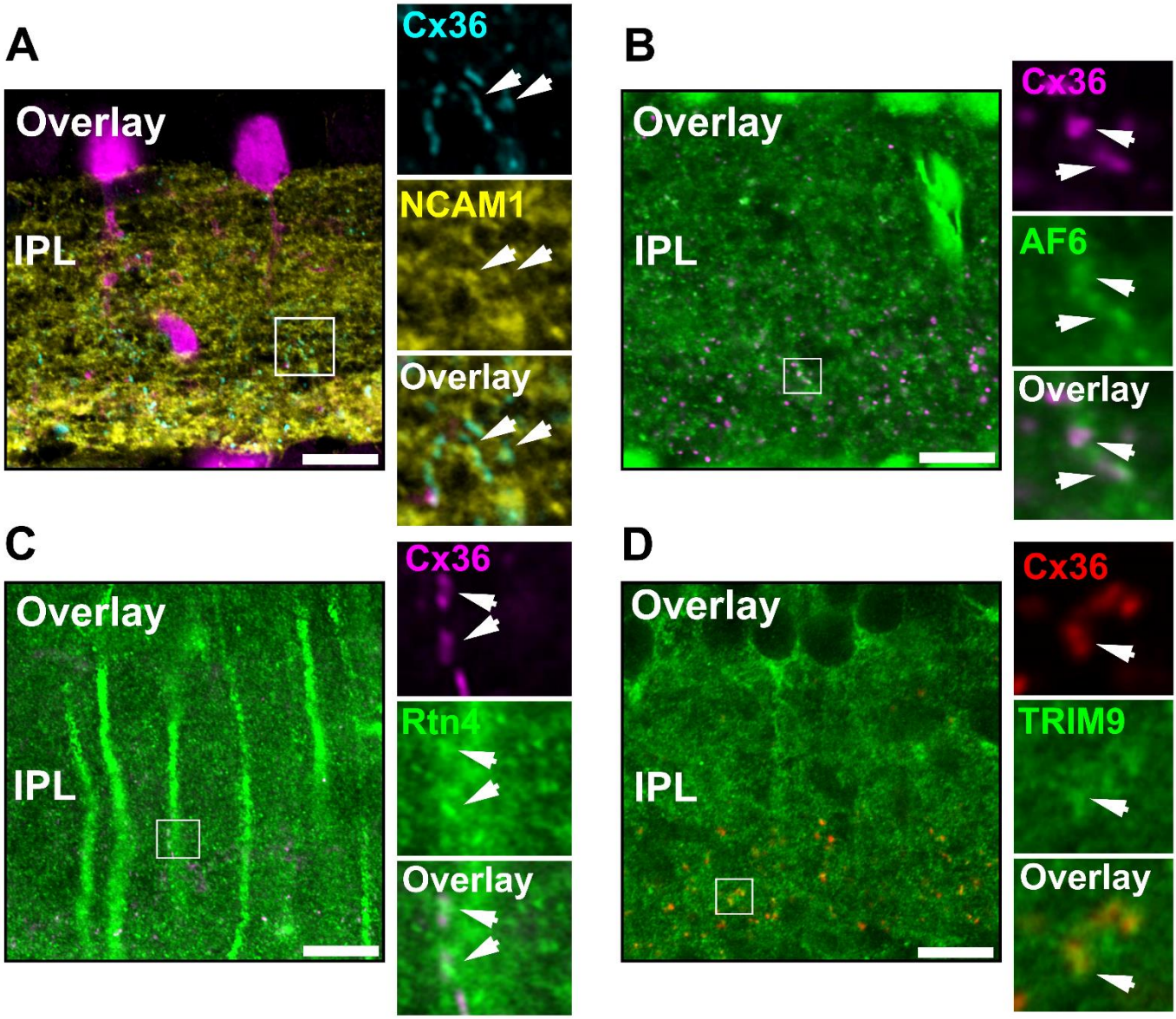

Supplementary figure 3

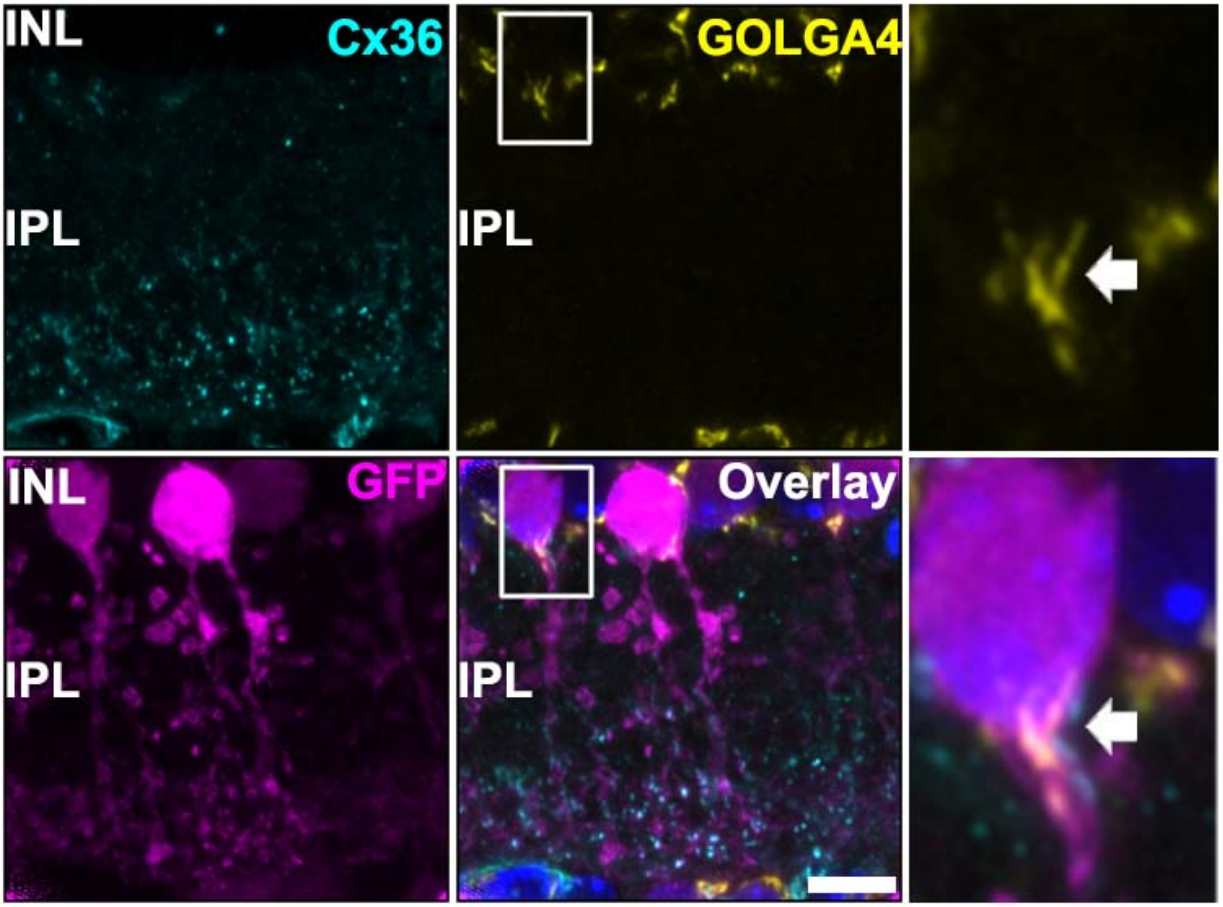

1045 **Supplementary figure 4**

1046
1047
1048
1049
1050
1051
1052
1053
1054
1055
1056
1057
1058
1059
1060

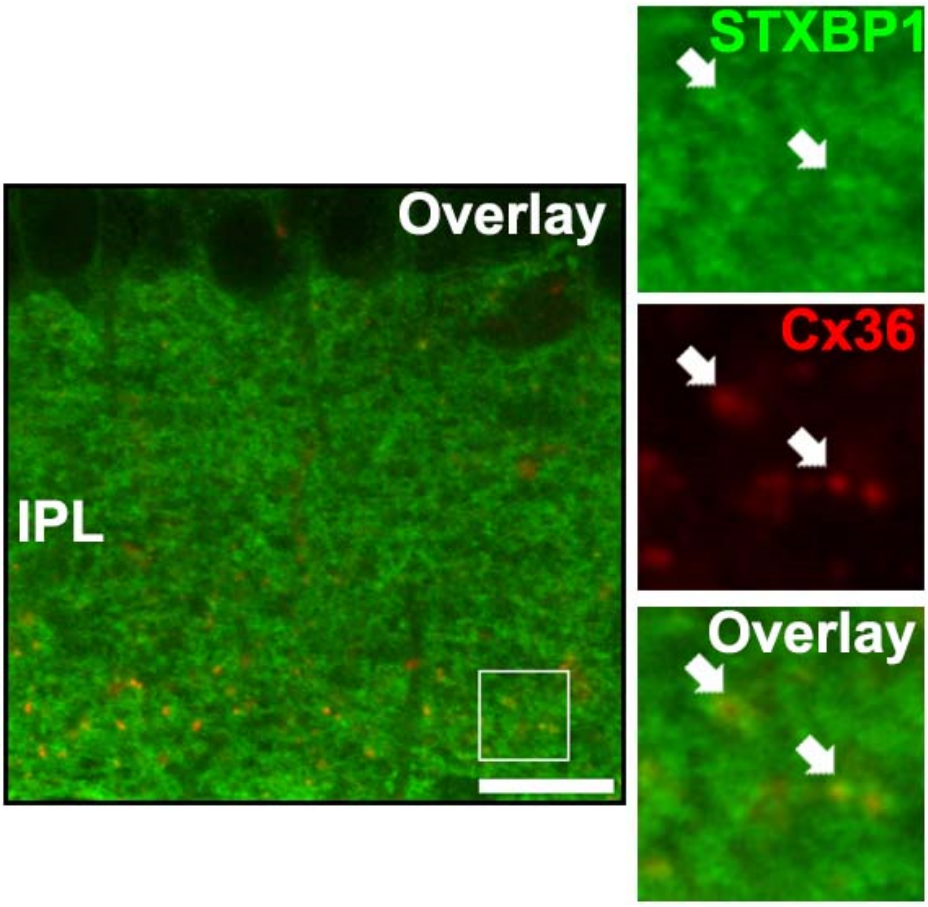

1061
1062
1063
1064
1065
1066
1067
1068
1069
1070
1071
1072

1073 **Supplementary figure 5**

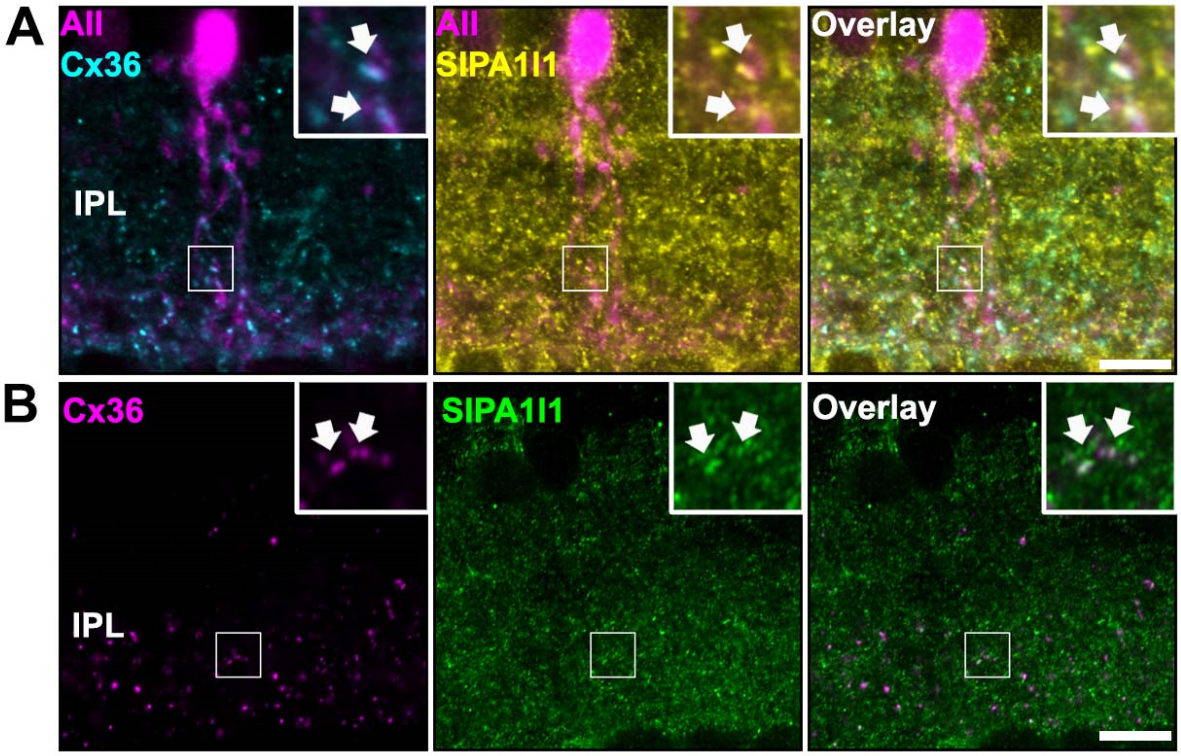

1074

1075

1076

1077

1078

1079

1080

1081

1082

1083

1084

1085

1086

1087

1088

References

1. M. V. Bennett, Electrical synapses, a personal perspective (or history). *Brain research reviews* **32**, 16-28 (2000).
2. C. Sotelo, The history of the synapse. *The Anatomical Record* **303**, 1252-1279 (2020).
3. E. A. Martin, A. M. Lasseigne, A. C. Miller, Understanding the molecular and cell biological mechanisms of electrical synapse formation. *Frontiers in neuroanatomy* **14**, 12 (2020).
4. T. C. Süudhof, Neurotransmitter release. *Pharmacology of Neurotransmitter Release*, 1-21 (2008).
5. M. J. Vaughn, J. S. Haas, On the diverse functions of electrical synapses. *Frontiers in Cellular Neuroscience* **16**, 910015 (2022).
6. S. G. Hormuzdi, M. A. Filippov, G. Mitropoulou, H. Monyer, R. Bruzzone, Electrical synapses: a dynamic signaling system that shapes the activity of neuronal networks. *Biochimica et Biophysica Acta (BBA)-Biomembranes* **1662**, 113-137 (2004).
7. G. Söhl, K. Willecke, Gap junctions and the connexin protein family. *Cardiovascular research* **62**, 228-232 (2004).
8. D. F. Condorelli, N. Belluardo, A. Trovato-Salinaro, G. Mudò, Expression of Cx36 in mammalian neurons. *Brain Research Reviews* **32**, 72-85 (2000).
9. S. A. Bloomfield, B. Völgyi, The diverse functional roles and regulation of neuronal gap junctions in the retina. *Nature Reviews Neuroscience* **10**, 495-506 (2009).
10. V. Serre-Beinier *et al.*, Cx36 makes channels coupling human pancreatic β-cells, and correlates with insulin expression. *Human molecular genetics* **18**, 428-439 (2009).
11. M. Srinivas *et al.*, Functional properties of channels formed by the neuronal gap junction protein connexin36. *Journal of Neuroscience* **19**, 9848-9855 (1999).
12. J. O'brien, The ever-changing electrical synapse. *Current opinion in neurobiology* **29**, 64-72 (2014).
13. W. W. Kothmann *et al.*, Nonsynaptic NMDA receptors mediate activity-dependent plasticity of gap junctional coupling in the AII amacrine cell network. *Journal of Neuroscience* **32**, 6747-6759 (2012).
14. W. W. Kothmann, S. C. Massey, J. O'Brien, Dopamine-stimulated dephosphorylation of connexin 36 mediates AII amacrine cell uncoupling. *Journal of Neuroscience* **29**, 14903-14911 (2009).
15. A. Feigenspan, B. Teubner, K. Willecke, R. Weiler, Expression of neuronal connexin36 in AII amacrine cells of the mammalian retina. *Journal of Neuroscience* **21**, 230-239 (2001).
16. R. E. Marc, J. R. Anderson, B. W. Jones, C. L. Sigulinsky, J. S. Lauritzen, The AII amacrine cell connectome: a dense network hub. *Frontiers in neural circuits* **8**, 104 (2014).
17. C. Del Corsso, R. Iglesias, G. Zoidl, R. Dermietzel, D. C. Spray, Calmodulin dependent protein kinase increases conductance at gap junctions formed by the neuronal gap junction protein connexin36. *Brain research* **1487**, 69-77 (2012).
18. C. Alev *et al.*, The neuronal connexin36 interacts with and is phosphorylated by CaMKII in a way similar to CaMKII interaction with glutamate receptors. *Proceedings of the National Academy of Sciences* **105**, 20964-20969 (2008).
19. J. Lisman, H. Schulman, H. Cline, The molecular basis of CaMKII function in synaptic and behavioural memory. *Nature Reviews Neuroscience* **3**, 175-190 (2002).
20. A. A. Coley, W.-J. Gao, PSD95: A synaptic protein implicated in schizophrenia or autism? *Progress in Neuro-Psychopharmacology and Biological Psychiatry* **82**, 187-194 (2018).
21. S. P. Cárdenas-García, S. Ijaz, A. E. Pereda, The components of an electrical synapse as revealed by expansion microscopy of a single synaptic contact. *Elife* **13**, e91931 (2024).

22. A. C. Miller, A. E. Pereda, The electrical synapse: molecular complexities at the gap and beyond. *Developmental neurobiology* **77**, 562-574 (2017).
23. E. Strettoi, E. Raviola, R. F. Dacheux, Synaptic connections of the narrow-field, bistratified rod amacrine cell (AII) in the rabbit retina. *Journal of Comparative Neurology* **325**, 152-168 (1992).
24. K. J. Roux, D. I. Kim, M. Raida, B. Burke, A promiscuous biotin ligase fusion protein identifies proximal and interacting proteins in mammalian cells. *Journal of cell biology* **196**, 801-810 (2012).
25. T. C. Branon *et al.*, Efficient proximity labeling in living cells and organisms with TurboID. *Nature biotechnology* **36**, 880-887 (2018).
26. T. Takano *et al.*, Chemico-genetic discovery of astrocytic control of inhibition in vivo. *Nature* **588**, 296-302 (2020).
27. M. Artan *et al.*, Interactome analysis of Caenorhabditis elegans synapses by TurboID-based proximity labeling. *Journal of Biological Chemistry* **297** (2021).
28. A. Uezu *et al.*, Identification of an elaborate complex mediating postsynaptic inhibition. *Science* **353**, 1123-1129 (2016).
29. H. Y. Wang, Y.-P. Lin, C. K. Mitchell, S. Ram, J. O'Brien, Two-color fluorescent analysis of connexin 36 turnover: relationship to functional plasticity. *Journal of cell science* **128**, 3888-3897 (2015).
30. H. Li, A. Z. Chuang, J. O'Brien, Photoreceptor coupling is controlled by connexin 35 phosphorylation in zebrafish retina. *Journal of Neuroscience* **29**, 15178-15186 (2009).
31. H. Choi *et al.*, Analyzing protein-protein interactions from affinity purification-mass spectrometry data with SAINT. *Curr Protoc Bioinformatics* **Chapter 8**, 8 15 11-18 15 23 (2012).
32. X. Li, B. Lynn, J. Nagy, The effector and scaffolding proteins AF6 and MUPP1 interact with connexin36 and localize at gap junctions that form electrical synapses in rodent brain. *European Journal of Neuroscience* **35**, 166-181 (2012).
33. S. Tetenborg *et al.*, Phosphorylation of Connexin36 near the C-terminus switches binding affinities for PDZ-domain and 14–3–3 proteins in vitro. *Scientific reports* **10**, 18378 (2020).
34. A. M. Lasseigne *et al.*, Electrical synaptic transmission requires a postsynaptic scaffolding protein. *Elife* **10**, e66898 (2021).
35. C. Ciolofan *et al.*, Association of connexin36 and zonula occludens-1 with zonula occludens-2 and the transcription factor zonula occludens-1-associated nucleic acid-binding protein at neuronal gap junctions in rodent retina. *Neuroscience* **140**, 433-451 (2006).
36. J. O'Brien, H. B. Nguyen, S. L. Mills, Cone photoreceptors in bass retina use two connexins to mediate electrical coupling. *Journal of Neuroscience* **24**, 5632-5642 (2004).
37. Z. Xiong *et al.*, In vivo proteomic mapping through GFP-directed proximity-dependent biotin labelling in zebrafish. *Elife* **10**, e64631 (2021).
38. I. Helbig *et al.*, In vivo evidence for the involvement of the carboxy terminal domain in assembling connexin 36 at the electrical synapse. *Molecular and Cellular Neuroscience* **45**, 47-58 (2010).
39. A. Meyer *et al.*, AII amacrine cells discriminate between heterocellular and homocellular locations when assembling connexin36-containing gap junctions. *Journal of cell science* **127**, 1190-1202 (2014).
40. J. M. Christie *et al.*, Connexin36 mediates spike synchrony in olfactory bulb glomeruli. *Neuron* **46**, 761-772 (2005).
41. H. Khabou *et al.*, Optogenetic targeting of AII amacrine cells restores retinal computations performed by the inner retina. *Molecular Therapy-Methods & Clinical Development* **31** (2023).

1184 42. A. Feigenspan *et al.*, Expression of connexin36 in cone pedicles and OFF-cone bipolar cells
1185 of the mouse retina. *Journal of Neuroscience* **24**, 3325-3334 (2004).
1186 43. J. C. Tang *et al.*, Detection and manipulation of live antigen-expressing cells using
1187 conditionally stable nanobodies. *Elife* **5**, e15312 (2016).
1188 44. C. E. Flores *et al.*, Trafficking of gap junction channels at a vertebrate electrical synapse in
1189 vivo. *Proceedings of the National Academy of Sciences* **109**, E573-E582 (2012).
1190 45. B. Lynn, X. Li, J. Nagy, Under construction: building the macromolecular superstructure and
1191 signaling components of an electrical synapse. *The Journal of membrane biology* **245**, 303-
1192 317 (2012).
1193 46. C. E. Flores, X. Li, M. V. Bennett, J. I. Nagy, A. E. Pereda, Interaction between connexin35 and
1194 zonula occludens-1 and its potential role in the regulation of electrical synapses.
1195 *Proceedings of the National Academy of Sciences* **105**, 12545-12550 (2008).
1196 47. S. Tetenborg *et al.*, Trafficking of Connexin36 (Cx36) in the early secretory pathway. *bioRxiv*
1197 (2024).
1198 48. E. Leithe, S. Sirnes, T. Fykerud, A. Kjenseth, E. Rivedal, Endocytosis and post-endocytic
1199 sorting of connexins. *Biochimica et Biophysica Acta (BBA)-Biomembranes* **1818**, 1870-1879
1200 (2012).
1201 49. E. A. Martin *et al.*, Neurobeachin controls the asymmetric subcellular distribution of
1202 electrical synapse proteins. *Current Biology* **33**, 2063-2074. e2064 (2023).
1203 50. Y.-K. Tu, J. G. Duman, K. F. Tolias, The adhesion-GPCR BAI1 promotes excitatory
1204 synaptogenesis by coordinating bidirectional trans-synaptic signaling. *Journal of*
1205 *Neuroscience* **38**, 8388-8406 (2018).
1206 51. C. Hartmann *et al.*, The mitochondrial outer membrane protein SYNJ2BP interacts with the
1207 cell adhesion molecule TMIGD1 and can recruit it to mitochondria. *BMC Molecular and Cell*
1208 *Biology* **21**, 1-17 (2020).
1209 52. S. Tetenborg *et al.*, Regulation of Cx36 trafficking through the early secretory pathway by
1210 COPII cargo receptors and Grasp55. *Cellular and Molecular Life Sciences* **81**, 1-17 (2024).
1211 53. Y. Tsukamoto, N. Omi, Classification of mouse retinal bipolar cells: type-specific connectivity
1212 with special reference to rod-driven AII amacrine pathways. *Frontiers in neuroanatomy* **11**,
1213 92 (2017).
1214 54. J. Nagy, B. Lynn, Structural and intermolecular associations between connexin36 and protein
1215 components of the adherens junction–neuronal gap junction complex. *Neuroscience* **384**,
1216 241-261 (2018).
1217 55. J. O'Brien, R. Bruzzone, T. W. White, M. R. Al-Ubaidi, H. Ripps, Cloning and expression of two
1218 related connexins from the perch retina define a distinct subgroup of the connexin family.
1219 *Journal of Neuroscience* **18**, 7625-7637 (1998).
1220 56. A. Dolnik *et al.*, Sipa1l3/SPAR3 is targeted to postsynaptic specializations and interacts with
1221 the Fezzin ProSAPiP1/Lzts3. *Journal of Neurochemistry* **136**, 28-35 (2016).
1222 57. R. Greenlees *et al.*, Mutations in SIPA1L3 cause eye defects through disruption of cell polarity
1223 and cytoskeleton organization. *Human molecular genetics* **24**, 5789-5804 (2015).
1224 58. J. G. Duman *et al.*, The adhesion-GPCR BAI1 regulates synaptogenesis by controlling the
1225 recruitment of the Par3/Tiam1 polarity complex to synaptic sites. *Journal of Neuroscience*
1226 **33**, 6964-6978 (2013).
1227 59. M. Westerfield, *The zebrafish book: A guide for the laboratory use of zebrafish Danio ("*
1228 *Brachydanio Rerio")* (University of Oregon, 2007).
1229 60. A. Santhanam *et al.*, A zebrafish model of retinitis pigmentosa shows continuous
1230 degeneration and regeneration of rod photoreceptors. *Cells* **9**, 2242 (2020).

61. N. Jin *et al.*, Molecular and functional architecture of the mouse photoreceptor network. *Science advances* **6**, eaba7232 (2020).
62. S. Tetenborg *et al.*, Intralumenal docking of connexin 36 channels in the ER isolates mistrafficked protein. *Journal of Biological Chemistry* **299** (2023).
63. K. Matsuura *et al.*, SIPA1L1/SPAR1 interacts with the neurabin family of proteins and is involved in GPCR signaling. *Journal of Neuroscience* **42**, 2448-2473 (2022).
64. S. Tetenborg, E. Martinez-Soler, O. John, Characterizing ER Retention Defects of PDZ Binding Deficient Cx36 Mutants Using Confocal Microscopy. *Bio-protocol* **14**, e5034 (2024).
65. P. Shannon *et al.*, Cytoscape: a software environment for integrated models of biomolecular interaction networks. *Genome research* **13**, 2498-2504 (2003).
66. G. Bindea *et al.*, ClueGO: a Cytoscape plug-in to decipher functionally grouped gene ontology and pathway annotation networks. *Bioinformatics* **25**, 1091-1093 (2009).
67. D. Szklarczyk *et al.*, The STRING database in 2023: protein–protein association networks and functional enrichment analyses for any sequenced genome of interest. *Nucleic acids research* **51**, D638-D646 (2023).
68. S. Tetenborg *et al.*, Differential distribution of retinal Ca2+/calmodulin-dependent kinase II (CaMKII) isoforms indicates CaMKII-β and-δ as specific elements of electrical synapses made of connexin36 (Cx36). *Frontiers in molecular neuroscience* **10**, 425 (2017).
69. S. Tetenborg *et al.*, Localization of retinal Ca2+/calmodulin-dependent kinase II-β (CaMKII-β) at bipolar cell gap junctions and cross-reactivity of a monoclonal anti-CaMKII-β antibody with Connexin36. *Frontiers in Molecular Neuroscience* **12**, 206 (2019).
70. J. Schindelin *et al.*, Fiji: an open-source platform for biological-image analysis. *Nature methods* **9**, 676-682 (2012).
71. C. L. Sigulinsky, R. L. Pfeiffer, B. W. Jones, Retinal Connectomics: A Review. *Annual Review of Vision Science* **10**, 263-291 (2024).
72. J. R. Anderson *et al.*, A computational framework for ultrastructural mapping of neural circuitry. *PLoS biology* **7**, e1000074 (2009).
73. J. R. Anderson *et al.*, Exploring the retinal connectome. *Molecular vision* **17**, 355 (2011).
74. R. Marc, R. Murry, S. Basinger, Pattern recognition of amino acid signatures in retinal neurons. *Journal of Neuroscience* **15**, 5106-5129 (1995).